Rational runoff coefficient for rational formula

Giorgio Baiamonte

Department of Agricultural, Food and Forest Sciences (SAAF), viale delle Scienze, Edificio 4, 90128 Palermo, ITALY.

ABSTRACT

The Rational Formula (RF), also known as the CIA formula, is probably the most applied equation in practical hydrology to compute the peak discharge despite it's various drawbacks, due to its simplicity and effective compromise between theory and data availability. Thus, after more than a century, the estimation of peak discharge thought the RF is still an important and challenging aspect of engineering hydrology. The RF assumes the linearity of the hillslope response, neglects the time to ponding and the antecedent soil moisture condition, and requires estimating the critical duration of rainfall and of the runoff coefficient, which both are highly controversial. Moreover, the runoff coefficient is simply assumed to be return period-independent and event time-independent. This paper proposes an advanced rational formula that makes it possible to derive the peak discharge at the hill slope scale, where the above assumptions of the classical RF are relaxed. It is based on three simplified and more or less consolidated models: i) the Green-Ampt model for infiltration, ii) the kinematic wave model for infiltration excess transportation, and iii) the intensity-duration-frequency model to described the yearly maximum rainfall intensity, which of course also require assumptions. Physically based runoff coefficient tables, which however are not affected by subjectivity, are arranged and applications of the derived procedure are performed.

Keywords: rational formula, hydrologic response, hillslope scale, Green-Ampt model, runoff coefficient, kinematic wave.

1. Introduction

The science of hydrology holds a central role in the field of environmental Earth science, being intimately connected to meteorology, climatology, hydrogeology and ecology (Sivapalan, 2003, 2005). In particular, the knowledge of hillslope hydrology is fundamental for understanding flood phenomenon and for predicting peak discharge and its probability distribution, which is necessary in many practical applications (the design of hydraulic structures, as well as urban and extra-urban planning, etc.). The estimation of peak discharge and runoff values for use in designing certain hydraulic structures is still an important and challenging aspect of engineering hydrology (Viessman and Lewis 2003, Grimaldi and Petroselli, 2015).

In order to determine the peak discharge, under the Hortonian mechanism of runoff generation, the traditional approach of equating the critical duration of rainfall, t_{cr}, to the time of concentration, T_c, is usually addressed (Thompson, 2006). This assumption is valid for planes with low infiltration loss. In this case, the full plane area contributes to the maximum peak discharge (Chen and Wong, 1993). For planes with high infiltration loss (Baiamonte, 2016), the duration of the critical rainfall associated with the maximum peak discharge may be shorter than the time of concentration. Under this condition, only part of the plane contributes to the maximum peak discharge (Baiamonte and Agnese, 2016). However, under the Hortonian mechanism of runoff generation, when soils exhibit low permeability, the time of concentration for a watershed is widely used as a time parameter to estimate peak discharges in hydrologic designs. Fang et al. (2008) empirically estimated T_c for 96 Texas watersheds using five empirical equations: Williams (1922), Kirpich (1940), Johnstone–Cross (1949), Haktanir–Sezen (1990), and Simas–Hawkins (2002) methods. By using the NRCS velocity method, the Authors found that the average relative difference between the estimations of the time of concentration was 50% with peaks of 90%.

Grimaldi et al. (2012) demonstrated that available approaches to estimate T_c may yield numerical predictions that differ from each other by up to 500%.

Recently de Almeida et al. (2016) emphasized the lack of a universally accepted definition for this parameter. After an extensive bibliographic review, by using thirty empiric methodologies to estimate T_c and data from a rural watershed, Almeida et al. (2016) showed the variability of empiric methodologies used in its estimations.

The importance of T_c estimation is related to its use in the rational formula (RF) to determine the design rainfall. The rational formula dates back to the 1850s in Ireland (Mulvaney, 1851; Bedient and Huber, 1988) and it is still widely applied to analyze the peak discharge of a small basin for a rainfall of T_c duration, thus, under the assumption that the intensities of both rainfall and infiltration or loss are uniformly distributed in time and space. The RF success is likely due to multiple factors. The formula is very easy to apply, the input data is easy to obtain as the formula only requires the intensity–duration–frequency (IDF) curves, T_c and the runoff coefficient, *C*. Finally, the formula is not entirely empirical, and the concept of the critical rainfall is easy to understand and is persuasive (Grimaldi and Petroselli, 2015). Therefore, simplicity and its limited data requirements motivate why it is still applied, investigated and interpreted.

In order to reduce the subjectivity of the hydrologist in the RF application, Grimaldi and Petroselli, (2015) introduced a rainfall excess estimation method (CN4GA), which makes it possible to use the curve number, *CN*, instead of *C*, and the use of an appropriately adapted geomorphological unit hydrograph (WFIUH-1par). A comparison between RF and the alternative procedure showed that the latter overestimates the peak and that the RF underestimates it. Moreover, the Authors showed that the RF in its original formulation leaves the practitioner too much freedom in its application because the original *C* tables provide a range of values with a poor classification of soil properties.

Wijesinghe and Wijesekera (2011) showed that the Unit Hydrograph can be derived using the peak discharge obtained from the RF and the unit depth of rainfall in calculating the rainfall

intensity. The Authors took into account possible alternatives for selecting sub catchments and the selection of a guideline to determine C and the T_c. Wijesinghe and Wijesekera (2011) found a significant variation of the results with the selected alternatives.

Recently, Wang and Wang (2018) developed the Rational Method Prime (RMP) that follows the basic principle of the RF but instead recalculates catchment variables by taking into account runoff control effects and evaluates runoff control efficiencies by using two indices. The Authors recognized three merits in the suggested RMP: (1) it provides an integrated response of the whole catchment with runoff controls; (2) it interprets runoff control effects by plotting runoff flow rate-rainfall duration curves; and (3) it connects the design of runoff controls and storm sewers that are based on different design principles and rainfall statistics. Case study results showed that runoff controls reduced peak flow rates in a wide range by 5.8-92%, corresponding to reduction factors for the return period of the maximum flow rate from 0.04 to 0.76. Like Grimaldi and Petroselli (2015), Wang and Wang (2018) also showed that the original RF is based on many assumptions, which also cause its weakness.

Whatever the criterion of T_c estimation is, the use of RM also involves the C estimation, which is a crucial point when one wants to determine the peak discharge. Indeed, errors in computing C linearly influence the peak discharge.

Advancements in the C empirical estimations have resulted in many reliable experimental efforts (Dhakal et al., 2012; Dhakal et al., 2013; Grillone et al., 2014). Recently, Dhakal et al. (2012) found that C values derived from the two data sets were essentially the same for 90 watersheds in Texas and by using land-use/land cover (LULC) data for 1992 and 2001. Volumetric runoff coefficients (C_v) were estimated by using observed rainfall and runoff depths from more than 1,600 events observed in the watersheds. Watershed-median and watershed average Cv values were computed, and both are consistent with data from the National Urban Runoff Program (NURP), which had 20 projects to study pollutants from 76 U.S. urban watersheds, with drainage areas ranging from 0.004 to 115 km^2 (USEPA 1983). Two regression equations of C_v versus percent

104 impervious area were developed and combined into a single equation that can be used to
105 empirically estimate C_v values for similar Texas watersheds.

106 A well-accepted practice consists in considering C return period-dependent, which was not
107 considered in the original RF. Dhakal et al. (2013) derived rate-based runoff coefficients as a
108 function of the return period, $C(T)$, for 36 undeveloped watersheds in Texas using peak discharge
109 frequency from previously published regional regression equations and rainfall intensity frequency
110 for return periods T of 2, 5, 10, 25, 50, and 100 years. The $C(T)$ values and return period
111 adjustments $C(T)/C(T = 10 \text{ years})$ determined in their study are most applicable to undeveloped
112 watersheds.

113 Tay and Afshar (2014) compared computed C using a linear empirical method with the runoff
114 coefficient assigned for different land use and surface type, revealing that the linear empirical
115 formula gives reliable results. The Authors justified their findings of a smaller value of the C
116 coefficient because the RF is limited to a watershed area equal to 80 hectares or smaller, and
117 evaluated the dependency of the rational formula runoff coefficients on the return period for two
118 locations in Texas.

119 Froehlich (2016) developed numerical solutions for dimensionless peak discharge in the form
120 of graphical relationships, and also as mathematical expressions that approximated the graphs
121 closely. Comparing peak discharge found by the proposed approach to the rational formula
122 provided a means of evaluating the relationship between runoff coefficients and rainfall return
123 periods. When compared to runoff coefficient adjustment factors found by others for 36
124 undeveloped watersheds in Texas, the return period adjustment factors calculated by Froehlich
125 (2016) illustrated a large difference that result because of the wide variability of parameters that
126 influence small catchment runoff (such as precipitation, soils, and land-surface cover) within a
127 region as vast as Texas.

128 However, Chin (2017) showed that Froehlich (2016) equated the incremental rainfall excess
129 within each time interval to the incremental runoff predicted by the Natural Resources Conservation

Service (NRCS) curve-number model when calculating the runoff hydrograph, and this could give physically unrealistic results (e.g., Chin 2013; Morel-Seytoux and Verdin 1981).

In conclusion, the issue of empirically-based peak discharge estimation is widely argued and a need for simple, yet adaptive modeling guidelines for engineers and researchers using these tools still exists, specifically for ungauged basins where no series discharge and runoff data is available. Indeed, although many definitions and estimation procedures to determine the peak discharge can be found in the technical literature, a universally accepted definition of a physically based peak discharge and of the related time of concentration is not known.

With reference to physically based approaches, there have been a multitude of studies on the hydrologic response at the hill slope scale. One approach for deriving the hillslope response utilizes, in a distributed form, the differential equations of unsteady overland flow, specifically developed at the hydrodynamic scale, in order to account for the spatial heterogeneity of soil characteristics, topography, roughness, and vegetation cover on the hillslope (Baiamonte et al., 2014; Baiamonte et al., 2017). This approach seemingly mimics the complete hydraulics of flow. However, the very complex patterns generated by spatial heterogeneity can cause considerable doubts in the prediction of hillslope response (Cundy and Tento, 1985, Sivapalan, 2003; Blöschl et al., 2013), even by very sophisticated approaches.

Sivapalan (2003) stated that “the root cause of the difficulties is the tremendous heterogeneity of the land surface condition, soils, vegetation, land use, etc., and the space–time variability of climatic inputs, occurring over a wide range of space and time scales. The heterogeneity is pervasive, and never seems to disappear at whatever scale we observe, ranging from largescale geological formations, the soil catena at hillslope and basin scales, down to the macropores that are ubiquitous at the plot scale”. Sivapalan (2003) also emphasized that theory development will only advance if we can develop simple models (which may be mere caricatures of the basin system). As theory advances, the simple models will give way to the development and

155 testing of more complex ones that capture more of the essential characteristics of real hillslopes and
156 basins.

157 Recently, in agreement with this line of thinking and under constant rainfall intensity,
158 Baiamonte and Singh (2016a) derived the hillslope time of concentration, T_c, by combining two
159 simplified, well-known and more or less consolidated models, i) the Green-Ampt model to account
160 for infiltration and ii) the kinematic wave to model the rainfall excess transportation. The solutions
161 were valid under the Horton's mechanism of runoff production, which is typical of arid and
162 semiarid regions, generally characterized by short duration, high rainfall intensities and by
163 hillslopes without significant vegetation cover (Agnese et al., 2011; 2014). Baiamonte and Singh
164 (2016b) also derived T_c relationships for hillslopes of complex topography, which may present
165 concavity or convexity and that can be convergent or divergent. The same issue was previously
166 investigated by Agnese et al. (2001, 2017) who applied the non-linear storage model at the hillslope
167 scale rather than the kinematic wave model.

168 Recently Baiamonte and Singh (2017) derived a simplified analytical solution for the
169 probability distribution of peak discharge (GABS model) under the assumption that the runoff
170 generation is mainly Hortonian, starting from the above-mentioned Baiamonte and Singh (2016a),
171 where the hillslope response was limited to constant rainfall intensity. Thus, the infiltration process
172 is governed by the well-known Green-Ampt equation, whereas the rainfall excess transportation
173 was modelled by the kinematic wave. In particular, the Authors by introducing the IDF curves in
174 Baiamonte and Singh (2016a) to describe the maximum rainfall intensity, employed a line of
175 physically based approaches that have not been attempted before, giving rise to a unique probability
176 distribution of peak discharge for infiltrating hillslopes, based on measurable parameters (Agnese et
177 al., 2016).

178 The objective of this paper is to show that this kind of approach may lead to an advanced
179 rational formula at the hillslope scale where all of the issues previously described regarding the
180 limits in using the classical RF are removed. The suggested procedure accounts for the physical soil

hydrology of the hillslope and for the statistical hydrology describing rainfall events according to the IDF model for computing the design rainfall intensity. Thus, all parameters can be estimated from known or measurable physical characteristics and subjectivity in peak discharge estimation is relaxed. It accounts for the non-linearity of the hillslope response, which needs to be considered especially for small basins (Robinson et al. 1995; Ostrowski, 2003), and for *C* event time-dependence and return period-dependence. The *C* evaluation is not affected by personal evaluations and involves a critical duration of rainfall that is linked to the simultaneous infiltration and transportation processes. Physically based runoff coefficient tables are arranged and applications are performed.

2. Theory

2.1 Unsaturated soil condition

By using the kinematic wave model, first introduced for impervious hillslopes (Woolhiser and Liggett 1967), and the Green-Ampt infiltration model (Green and Ampt, 1911), Baiamonte and Singh (2016a) showed that if a rainfall intensity, i (m/s), of indefinite duration is applied to a hillslope of known geometry, the time of equilibrium, t_{eq} (s), can occur in the 1st or in the 2nd domain ($t_{eq} < t_k$ or $t_{eq} \geq t_k$, respectively) of the kinematic plane, depending on the normalized kinematic wave arrival time, τ_k, and the associated normalized infiltration capacity, f_{*k}:

$$\begin{cases} \tau_k = \dfrac{t_k}{t_c} = \tau_p + \dfrac{\rho^{-1}}{\left(f_{*k} - \rho^{-1}\right)} - \dfrac{\rho^{-1}}{\left(1 - \rho^{-1}\right)} + \psi_k \\ f_{*k} = \dfrac{f_k}{i} = 1 - \dfrac{\left(1 - \rho^{-1}\right)\left(f_{*k} - \rho^{-1}\right)^2}{\left(f_{*k} + 1 - 2\rho^{-1}\right)\rho^{-2}} \left(\tau_{eq,i}^2 - \dfrac{2\rho^{-1}\psi_k}{f_{*k} - \rho^{-1}} - \psi_k^2 \right) \end{cases} \quad (1)$$

where $\rho = i/K_s$, is the rainfall intensity normalized with respect to saturated hydraulic conductivity, K_s (mm/h), whereas the dimensionless group Ψ_k equals:

$$\psi_k = ln\left(\frac{i\left(f_k - K_s\right)}{f_k\left(i - K_s\right)}\right) \quad (2)$$

In Eq. (1), τ_p is the time to ponding, t_p (s), according to Green-Ampt infiltration model:

$$\tau_p = \frac{t_p}{t_c} = \frac{1}{\rho\left(\rho - 1\right)} \quad (3)$$

which is normalized, as well as the time t_k, with respect to the sorptivity time scale, t_c (s):

$$t_c = \frac{\theta_s \psi_m}{K_s}\left(1 - s\right) = \omega\left(1 - s\right) \quad (4)$$

where θ_s (m^3 m^{-3}) is the saturated volumetric water content, ψ_m (m) is the matric potential at the wetting front. In Eq. (4), t_c is rewritten in order to consolidate the soil hydrological parameters θ_s, ψ_m and K_s, in a characteristic time of the infiltration process, ω (s), independently of the antecedent soil moisture content (ASMC), which is expressed as saturation degree, s, in the right hand.

In Eq. (1), $\tau_{eq,i}$ is a parameter synthesizing both the hillslope geometry and soil hydrological characteristics, and equals the ratio between the time to equilibrium for an impervious hillslope, $t_{eq,imp}$, and the sorptivity scale, t_c:

$$\tau_{eq,i} = \frac{t_{eq,imp}}{t_c} = \frac{1}{\omega\left(1 - s\right)\sqrt{k_* i}} \quad (5)$$

where k_* is another parameter synthetically accounting for the gross hillslope "geometry", which was first introduced by Robinson and Sivapalan (1996):

$$k_* = \frac{\sqrt{S_0}}{n_{Mann} L} \tag{6}$$

where L (m) is the length of the hillslope, S_0 is the slope, and n_{Mann} (s $m^{-1/3}$) is the Manning friction factor.

By introducing the intensity-duration-frequency (IDF) curves, Baiamonte and Singh (2017) showed that t_k not only separates the two domains where the time to equilibrium occurs but, for any probability of non-exceedance, also corresponds to the critical duration of rainfall, t_{cr} (s), i.e. the duration of rainfall for which the maximum discharge, q_{cr} (m/s), at the bottom of the hillslope is achieved (see Fig. 4, Baiamonte and Singh, 2017). Therefore, in Eq. (1), the subscript "*k*" could be replaced with the subscript "*cr*" that stands for critical conditions.

Assuming a simple scaling behavior of the rainfall intensity, i_{cr} with t_{cr}, and the equality in the probability distribution according to the $(n - 1)$ scaling exponent of the IDF curves:

$$i_{cr}(T) \overset{d}{=} t_{cr}^{n-1} a_T \tag{7}$$

where a_T (m/s) is the maximum hourly rainfall intensity of an assigned return period, T (years), Baiamonte and Singh (2017) derived the probability distribution of peak discharge, $P(q_{max})$, according to a denoted GABS model. Thus, the latter can be used under the assumption of Green-Ampt infiltration and for a hillslope defined by θ_s, K_s, ψ_m (i.e. ω), by ASMC (i.e. *s*), by L, n_{Mann}, S_0 (i.e., k_*) for which a rainfall intensity, according to Eq. (7), is applied.

For fixed soil (ω = 13.5 h), hillslope geometry (k_* = 0.143) and scaling exponent (n = 0.36), **Figure 1** illustrates an example of $P(q_{max})$ relationships, which interestingly show that the influence of ASMC on the peak discharge becomes less and less important as the event probability of non-exceedance, P, increases. Moreover, for a fixed probability, the effect of ASMC agrees with what would be expected, so one can move from the dry antecedent soil condition to the unsaturated condition, to saturated conditions and to impervious hillslope condition, which corresponds to the highest peak discharge, for any P.

Assuming unsaturated soil conditions, to derive an analytical runoff coefficient, C, according to the GABS model, in order to consolidate rainfall, soil and hillslope geometry into three parameters, it was necessary to change some parameters. In particular, the normalized rainfall intensity, ρ, the normalized infiltration capacity, f_{*k}, and the hillslope geometry parameter, k_*, appearing under constant rainfall intensity, in Eqs. (1) were rewritten as follows:

$$\rho = \frac{i}{K_s} \quad \rightarrow \quad \rho_T = \frac{a_T}{K_s} \tag{8a}$$

$$f_{*k} = \frac{f_k}{i} \quad \rightarrow \quad f_{*cr} = \frac{f_{cr}}{K_s} \tag{8a}$$

$$k_* = \frac{\sqrt{S_0}}{n_{Mann} L} \quad \rightarrow \quad k_* K_s^{-1} = \frac{\sqrt{S_0}}{n_{Mann} L K_s} \tag{8b}$$

Rearranging Eqs. (1), according to Eq. (7) and taking into account Eqs. (8), the system can be rewritten as a function of the three parameters ρ_T, t_c and $k_* K_s^{-1}$:

$$\begin{cases} t_{cr} = t_c \left(\dfrac{1}{f_{*cr} - 1} - \dfrac{1}{\rho_T \, t_{cr}^{n-1}} + \psi_{cr} \right) \\ f_{*cr} = \rho_T \, t_{cr}^{n-1} - \dfrac{\left(f_{*cr} - 1\right)^2 \rho_T \, t_{cr}^{n-1} \left(\rho_T \, t_{cr}^{n-1} - 1\right)}{\rho_T \, t_{cr}^{n-1} + f_{*cr} - 2} \left(\dfrac{1}{\left(k_* \, K_s^{-1}\right) \rho_T \, t_{cr}^{n-1} \, t_c^2} - \dfrac{2\psi_{cr}}{f_{*cr} - 1} - \psi_{cr}^2 \right) \end{cases} \tag{9}$$

with the Ψ_{cr} parameter expressed as:

$$\psi_{cr} = ln\left(\frac{1-f_{*cr}^{-1}}{1-\rho_T^{-1}\,t_{cr}^{1-n}}\right) \tag{10}$$

Usefully, the same parameters t_c, ρ_T and $k_*\ K_s^{-1}$ also appear in the derivation of the runoff coefficient relationship reported below:

$$C = \frac{q_{cr}}{q_{cr,imp}} = \left(\left(k_*\ K_s^{-1}\ \rho_T\right)^{n/1+n}\ t_{cr}^{n-1}\ t_c\left(\frac{1-f_{*cr}\ \rho_T^{-1}\ t_{cr}^{1-n}}{f_{*cr}-1}+\Psi_{cr}\right)\right)^2 \tag{11}$$

It should be noted that the runoff coefficient differs from that defined in the classical rational formula where the peak discharge is expressed with respect to critical rainfall intensity. Indeed, in Eq. (11) the peak discharge is expressed with respect to the peak discharge, $q_{cr,imp}$, corresponding to an impervious hillslope with the same geometry (k_*), and rainfall (a_T) of the studying hillslope. The $q_{cr,imp}$ relationship for deriving Eq. (11) was expressed according to Baiamonte and Singh (2017, see Eq. 9 and Eq. 11):

$$q_{cr,imp} = k_*^{(1-n)/(1+n)}\ a_T^{2/(1+n)} \tag{12}$$

Of course, for an assigned triplet of values (ρ_T, t_c and $k_*\ K_s^{-1}$), using Eq. (11) requires solving the system of Eq. (9) in order to detect the critical duration of rainfall, t_{cr}, and the corresponding infiltration capacity, f_{*cr}, which also appear in it. Knowledge of Eq. (11) allows the important roles of rainfall, soil hydrological characteristics and hillslope geometry to be compacted in the

parameters ρ_T, t_c and $k_* K_s^{-1}$, respectively, in order to derive a runoff coefficients table in a matrix form. As an alternative, the following relationship could be used to directly detect the peak discharge:

$$q_{cr} = C\, q_{cr,imp} = \frac{\left(k_*\, K_s^{-1}\right) t_c^2}{K_s^{1-4/(1+n)}} \left(\frac{f_{*cr} - \rho_T\, t_{cr}^{n-1}\left(1 + \left(f_{*cr} - 1\right)\Psi_{cr}\right)}{f_{*cr} - 1} \right)^2 \qquad (13)$$

However Eq. (13) is less general than Eq. (11), since the saturated hydraulic conductivity appears in the $k_* K_s^{-1}$ parameter but also appears in the denominator.

Before deriving the runoff coefficient tables, some important relationships between the involved parameters were studied. For fixed ρ_T = 100 and n = 0.36, **Figure 2** shows the relationship of the normalized infiltration capacity, f_{*cr}, versus the critical duration of rainfall, t_{cr} (**Figure 2a**), and versus the temporal scale of the infiltration process, t_c (**Figure 2b**), with $k_* K_s^{-1}$ as a parameter. The figure shows that a non-monotonic behavior occurs. With reference to **Figure 2a**, for a fixed f_{*cr}, two critical durations and two temporal scales providing peak discharges could be defined. From a practical point of view, the falling limb of f_{*cr} versus t_{cr} is not very interesting, since it refers to a very long duration of rainfall that can be achieved for a rainfall intensity that attains the saturated hydraulic conductivity where $f_{cr} \sim K_s$. The latter consideration is supported by the limiting condition of the illustrated curves, which are represented by the dashed line with the equation $f_{*cr} = \rho_T\, t_{cr}^{n-1}$ (also reported).

Of course, for a fixed f_{*cr}, at increasing $k_* K_s^{-1}$, because of the slope increases or the decreases in the Manning roughness (smoother hillslopes) of the hillslope length, the critical duration of rainfall decreases. Similar considerations, in agreement with the t_c physical meaning, can be done for **Figure 2b** and for **Figure 3a**, which illustrates the corresponding critical duration versus t_c relationships.

For the purpose of this study, **Figure 3b** shows the most significant variable, i.e. the runoff coefficient C as a function of the soil characteristics, t_c. Interestingly, according to what C is expected to be in the range 0 – 1, and for the fixed hillslope geometry, with decreasing t_c, as an example, because there are decreases the soil porosity or increases in ASMC, C increases until it attains a limiting value, which is less than one, as expected.

This limiting condition corresponds to the saturated soil condition and will be inspected in the following section. Before studying the runoff coefficient for saturated soil conditions, some further relationships between the involved parameters in dimensional form are illustrated. Indeed, grouping the variables from one hand can help in detecting analytical solutions; on the other hand, it risks falling into losing the physical meaning in a meaningless range of the grouped variables.

For $\rho_T = 100$, $n = 0.36$ and for just one value of $k_* K_s^{-1} = 0.25$, C coefficient relationships are reported versus the time dimension variables, t_p (Eq, 3), t_c (Eq, 4) and t_{cr} (Eq, 9) in **Figure 4a** and versus the flux dimension variable, f_{cr} (Eq, 9), i_{cr} (Eq, 7) and q_{cr} (Eq, 13) in **Figure 4b**. In the latter, the critical rainfall excess, $r_{cr} = i_{cr} - f_{cr}$ is also plotted, since it could be usefully compared with C versus i_{cr} and versus q_{cr} relationships, laying as expected in between them. For f_{cr}, the non-monotonic already discussed behavior appears, whereas in **Figure 4a** the time to ponding is inversely related to the C coefficient and as the rainfall duration increases, the runoff coefficient decreases.

2.2 Saturated soil condition ($s = 1$, $t_c = 0$, $f_{*cr} = 1$)

As observed above, the saturated condition is an important condition for the general solution (Eq. 9 and Eq. 11) since it represents its limiting condition and can be easier studied since it is not influenced by the sorptivity time scale, thus one less parameter occurs, giving that for $s = 1$, $t_c = 0$ (Eq. 4).

For this particular case, from the beginning of the rainfall, the peak discharge can be written by using the relationship introduced by Baiamonte and Agnese (2010, see Eq. 11) also used by Baiamonte and Singh (2016a, Eq. 3b) and Baiamonte and Singh (2016b, Eq. 31), and subtracting K_s from the rainfall (Eq. 7), because of the steady state infiltration:

$$q_{cr} = k_* \left(a_T \, t_{cr}^{n-1} - K_s\right)^2 t_{cr}^2 \tag{14}$$

For impervious hillslope, the corresponding critical duration of rainfall can be derived by imposing that q_{cr} matches the critical rainfall intensity minus K_s in Eq. (14), yielding:

$$t_{cr} = \frac{1}{\sqrt{k_* \left(a_T \, t_{cr}^{n-1} - K_s\right)}} \tag{15}$$

Eq. (15) can be rewritten by introducing the ρ_T parameter and showing that an asymptotic critical duration of rainfall occurs:

$$t_{cr} = \frac{1}{\sqrt{k_* \, K_s \left(\rho_T \, t_{cr}^{n-1} - 1\right)}} \quad \text{with} \quad t_{cr} < \frac{1}{\rho_T^{1/(n-1)}} \tag{16}$$

Eq. (16) is implicit in t_{cr}, but it can be made explicit with respect to the geometry parameter $k_* K_s$, which however differs from that previously introduced ($k_* K_s^{-1}$, Eq. 8b):

$$k_* \, K_s = \frac{1}{t_{cr}^2 \left(\rho_T \, t_{cr}^{n-1} - 1\right)} \tag{17}$$

For n = 0.36, Eq. (17) is plotted in **Figure 5a** as a function of t_{cr}, with ρ_T as a parameter. The figure shows that, similarly to **Figure 2a**, although with reference to f_{*cr}, a value of the critical duration, denoted as maximum, $t_{cr,max}$, occurs. In this simple case, putting the partial derivative of Eq. (6b) as equal to zero with respect to t_{cr}, yields:

$$\frac{d\left(k_* K_s\right)}{d\, t_{cr}} = \frac{2\, t_{cr} - \left(1+n\right)\rho_T\, t_{cr}^{n}}{t_{cr}^{2}\left(t_{cr} - \rho_T\, t_{cr}^{n}\right)^{2}} = 0 \qquad (18)$$

Eq. (18) makes it possible to detect the maximum value of the critical duration of rainfall, $t_{cr,max}$:

$$t_{cr,max} = \left(\frac{\rho_T\left(1+n\right)}{2}\right)^{1/1-n} \qquad (19)$$

By substituting Eq. (19) in Eq. (17), the corresponding minimum value of k_*K_s, $(k_*K_s)_{min}$, can be derived:

$$\left(k_* K_s\right)_{min} = \frac{\left(1+n\right)^{\left(n+1\right)/\left(n-1\right)}}{1-n}\left(\frac{\rho_T}{2}\right)^{2/\left(n-1\right)} \qquad (20)$$

Eq. (20), plotted in **Figure 5a**, splits the rising and the falling limbs of the k_*K_s versus t_{cr} relationships. For the rising limbs ($t_{cr} > t_{cr,max}$) and for any ρ_T value, at increasing k_*K_s, the k_*K_s versus t_{cr} function quickly approaches the vertical asymptote with the equation $t_{cr,asym} = \rho_T^{(1/1-n)}$ (see Eq. 16). As an example, the latter is illustrated in **Figure 5b**, for ρ_T = 50 (dash dot line).

As for unsaturated soil conditions, deriving the C coefficient for s = 1 requires that the peak discharge (Eq. 14) can be rewritten as a function of ρ_T by substituting Eq. (16) in Eq. (14):

$$q_{cr} = K_s\left(\rho_T\, t_{cr}^{n-1} - 1\right) \tag{21}$$

Thus, the C coefficient, as for the unsaturated soil conditions, can be derived as the ratio between the peak discharge for saturated condition (Eq. 21) and that for impervious hillslopes (Eq. 12):

$$C = \frac{q_{cr}}{q_{cr,imp}} = \frac{\rho_T\, t_{cr}^{n-1} - 1}{\left(k_*\, K_s\right)^{(1-n)/(1+n)}\, \rho_T^{2/(1+n)}} \tag{22}$$

Eq. (22) is plotted in **Figure 5b**, which shows a similar non-monotonic behavior of the C coefficient versus the geometry parameter, $k_*\, K_s$, i.e. compared to that reported in **Figure 3b**, although versus t_c.

Interestingly, the C value corresponding to $(k_*K_s)_{min}$, $C((k_*K_s)_{min})$, which can be derived by combining Eq. (22), Eq. (19) and Eq. (20), is independent on ρ_T parameter, and only depends on the rainfall structure, n:

$$C\left(\left(k_*\, K_s\right)_{min}\right) = \left(\frac{1-n}{2}\right)^{\frac{2}{1+n}} \tag{23}$$

Eq. (23) is reported in **Figure 5b**, verifying this occurrence. The knowledge of $C((k_*K_s)_{min})$ allows plotting, for saturated conditions, the C coefficient as a function of the rainfall (ρ_T) and hillslope geometry parameter ($k_*\, K_s$), in the C range, useful from a practical point of view ($C \geq C((k_*K_s)_{min})$), in order to also study the influence of the rainfall structure in the runoff coefficient.

The runoff coefficient C, according to Eq. (22), is plotted in **Figure 6** for different rainfall structure values (n = 0.2 - 0.52, step 0.04) and covering most of the practical k_*K_s, ρ_T , n and C values. Two different views were represented. **Figure 6a** shows that the obtained C surfaces for

high ρ_T values, whereas **Figure 6b** shows the C surfaces for low ρ_T values. Inspection of **Figure 6** leads to the following conclusion in agreement with what is expected. i) For high ρ_T values and for low $k_* K_s$ values, C increases with the rainfall structure (see the illustrated case in **Figure 6a**, $k_* K_s = 10^{-5}$, $\rho_T = 44.5$); ii) for low ρ_T values C is independent of the rainfall structure (see the illustrated case in **Figure 6b**, $k_* K_s = 10^{-5}$, $\rho_T = 2.5$). However, iii) the influence of n on C coefficient becomes less and less evident as $k_* K_s$ increases, for any ρ_T value, meaning that the quicker the hillslope response is, the smaller the influence of the rainfall structure is; iv) the increasing trend of C with n slightly reverses for high $k_* K_s$ values, as can be observed in **Figure 6a**, where for $n = 0.2$ the dark C surface is highlighted.

3. Runoff coefficient tables

As previously stated, the saturated soil condition is important, since it represents the limiting condition of the general C runoff coefficient solution (Eq. 11). The latter, for $n = 0.36$, is reported in **Figure 7**, as a function of the soil parameter (t_c), and for different ρ_T and $k_* K_s^{-1}$ values. C relationships belonging to the same ρ_T values are grouped by oval symbols. As expected with increasing ρ_T, C increases and, for fixed ρ_T, C increases with $k_* K_s^{-1}$, since the response of the hillslope becomes faster and faster.

For $\rho_T = 1$ ($k_* K_s^{-1} = 25$ and 5) and for $\rho_T = 5$ ($k_* K_s^{-1} = 25$ and 0.05) the limiting condition represented by the C runoff coefficient of the saturated condition (horizontal lines, Eq. 22) is plotted. As can be observed, the C coefficient for unsaturated soil conditions (Eq. 11) approaches to the limiting saturated soil condition ($t_c \sim 0$) as the t_c parameter decreases, for example because of ASMC increases ($s \sim 1$). The described occurrence in a certain sense validates the approach followed to derive Eq. (11, for $0 \leq s \leq 1$) as well as Eq. (12, for $s = 1$).

436 Similar considerations are valid for **Figure 8** where, for ρ_T = 10 and n = 0.36, the C
437 coefficient for unsaturated soil conditions (Eq. 11) is plotted versus $k_* K_s^{-1}$ and versus the critical
438 duration of rainfall, t_{cr}, normalized with respect to the asymptotic t_{cr} value, $t_{cr,asym} = \rho_T^{(1/1-n)}$.

439 The C coefficient for both the unsaturated (Eq. 11) and saturated soil conditions (Eq. 22), can
440 also be expressed as a function of the ratio $t_{*cr} = t_{cr}/t_{cr,asym}$, thus making it possible to simplify the C
441 coefficient solutions. In particular, for the unsaturated case both C coefficient and the peak
442 discharge can be rewritten as:

443

444 $$C = \frac{q_{cr}}{q_{cr,imp}} = \frac{\left(k_* K_s^{-1}\right)^{\frac{2n}{1+n}} \left(t_{*c} - t_{*cr}^n \left(f_{*cr} - 1\right)\right)^2}{\rho_T^{\frac{4n}{n^2-1}} \left(f_{*cr} - 1\right)^2} \quad (24)$$

445 $$q_{cr} = \frac{k_* K_s^{-1} \left(t_{*c} - t_{*cr}^n \left(f_{*cr} - 1\right)\right)^2}{\rho_T^{\frac{2}{n-1}} \left(f_{*cr} - 1\right)^2} K_s^{\frac{2}{1+n}} \quad (25)$$

446

447 where t_{*c} is the t_c parameter that has also been normalized with respect to $t_{cr,asym}$ ($t_{*c} = t_c/t_{cr,asym}$).
448 Whereas, for saturated soil conditions, C expressed as a function of t_{*cr} yields:

449

450 $$C = \frac{q_{cr}}{q_{cr,imp}} = \frac{t_{*cr}^{n-1} - 1}{\left(k_* K_s\right)^{(1-n)/(1+n)} \rho_T^{2/(1+n)}} \quad (26)$$

451

452 where the corresponding t_{cr} (Eq. 16) can also be expressed in a dimensionless form:

453

454 $$t_{*cr} = \frac{1}{\rho_T^{1/(1-n)} \sqrt{k_* K_s \left(t_{*cr}^{n-1} - 1\right)}} \quad (27)$$

455

Eq. (26) is also plotted in **Figure 8**, together with Eq. (24), showing a C tendency similar to that illustrated in **Figure 7**. From **Figure 8**, it seems that the general solution better approaches the limiting condition for low $k_* K_s^{-1}$ and high t_{cr} than vice versa.

Finally, it should be noted that, although the geometry parameter differs in both C formulations, $k_* K_s^{-1}$ in Eq. 11 for $0 \leq s \leq 1$, and $k_* K_s$ in Eq. 22 for $s = 1$, the latter matches the limiting condition of the general solution as well, since for unit K_s the geometry parameter becomes equal.

The high variability of the parameters involved in C estimation (more for $k_* K_s^{-1}$ and t_c than ρ_T), limits the use of the C plot reported in **Figure 7**, where a different order of magnitude of the involved parameters were considered. Towards the aim to attempt a framework useful for practical applications, for the fixed $n = 0.36$ considered above, a runoff coefficient table was structured.

According to the limited range of variability of the C coefficient (0 – 1), the table was organized for fixed C values rounded to one decimal place, and for different rainfall and hillslope geometry parameters. Following the $k_* K_s^{-1}$ and ρ_T ranges of variability explored in **Figure 8**, for fixed $k_* K_s^{-1}$ and ρ_T values, **Table 1** reports the corresponding t_c values.

Using **Table 1** first requires determining ρ_T value, meaning that a statistical analysis to check a simple scaling behavior of the IDF curves (Eq. 7) and, for a fixed return period, T, a_T estimation should be performed. Once K_s for the hillslope is selected (or measured), ρ_T reported in column can be entered. Measuring hillslope length and slope, Manning coefficient estimation allows calculating k_* (Eq. 6) and then $k_* K_s^{-1}$ to be entered in row. Measuring or estimating soil porosity, θ_s, ψ_m, according to texture and structure of the soil, and assuming AMSC, allows calculating t_c (Eq. 4), which corresponds to a C runoff coefficient value. Log-Log regression could be considered, if the actual t_c value is far and in between two contiguous t_c values reported in **Table 1**, for the assigned coefficient ρ_T and $k_* K_s^{-1}$. Bold values in circular brackets reported in **Table 1** correspond to the runoff coefficient C of the saturated soil conditions ($s = 1$, $t_c = 0$), which of course give values less

481 than those (for unsaturated soil conditions) reported in the corresponding row, at the second column
482 from the left.
483
484 **4. Application and comparison with the CIA formula**
485
486 In this section, in order to list the implications of the described procedure for the runoff
487 coefficient that usually needs to be estimated when applying the rational formula (CIA), a
488 comparison with the latter has been performed.
489 Consider a hillslope with the geometric characteristics reported in **Table 2**. The slope equals
490 17.8%, the length is L = 466 m and the Manning coefficient was fixed n_{Mann} = 0.125 $m^{-1/3}$ s., K_s =
491 0.72 mm/h was assumed from the texture and structural characteristics of the soil, which gives $k_* K_s^{-1}$
492 = 0.01.
493 Assume that the mean soil hydrological characteristics are known, which usually present high
494 spatial variability even though the same land management (Papanicolaou et al., 2015; Cullotta et al.,
495 2016; Baiamonte et al., 2017); they are synthetically described by the parameters reported in **Table**
496 **2**, where for a dry ASMC (s = 0), the soil sorptivity time scale t_c equals around 151 h.
497 The application was carried out by using the maximum hourly intensity data-series of the
498 Acireale station (Sicily), whose location is reported in **Figure 9**. For the available high sample size
499 (N = 60), a simple scaling behavior was checked and a rainfall structural parameter n = 0.36 was
500 estimated (Baiamonte and D'Asaro, 2016). Also assume that one wants to determine the peak
501 discharge associated with a return period T = 15.4 years, so that the corresponding probability of
502 non-exceedance equals 0.94 (**Table 2**). The Gumbel distribution (EV1) fitted the hourly maximum
503 rainfall intensities well, and the a_T parameter was estimated according to the parameter α = 0.07
504 mm^{-1} and to the mode u = 32.4 mm/h, yielding a_T = 72.4 mm/h. As a consequence, $\rho_T = a_T / K_s$ =
505 100.

In conclusion, the triplet of parameters (ρ_T, t_c, $k_* K_s^{-1}$) needed to apply the suggested procedure are all known. For the values of these three parameters, **Table 1** provides a runoff coefficient C = 0.8, which needs to be multiplied for the peak discharge, corresponding to a hillslope with the same geometry, but impervious, $q_{cr,imp}$. The latter could be determined by Eq. (12), which is rewritten here, as a function of the two EV1 parameters u and α (Baiamonte and Singh, 2017):

$$q_{cr,imp} = \left(3.6\,k_*\right)^{(1-n)/(1+n)} \left(u - \frac{1}{\alpha} ln\left(ln \frac{T}{T-1} \right) \right)^{2/(n+1)} \tag{28}$$

where the 3.6 k_* factor makes it possible to express L in (m) and the Manning friction factor, n_{Mann}, in ($m^{-1/3}s$), u is expressed in (mm h^{-1}), α in (mm^{-1}) , in order to obtain $q_{cr,imp}$ in (mm h^{-1}). For the Acireale station, under conditions of an impervious hillslope and for T = 15.4 years, the application of Eq. (28) gives $q_{cr,imp}$ = 97.53 mm h^{-1}, which multiplied for C = 0.8 (Eq. 24, 26) gives, q_{cr} = C $q_{cr,imp}$ = 78.03 mm/h (2.02 m^3/s).

The corresponding critical duration of rainfall t_{cr}, Eq. (9), which is not requested if using the runoff coefficient table, for the sake of comparison with the CIA formula, is also reported in **Table 2** (t_{cr} = 0.46 h, f_{cr} = 9.75 mm/h).

Following the CIA formula, the critical duration of rainfall and the runoff coefficient should be estimated according to the time of concentration empirical relationships, which usually do not account for the selected return period, time to ponding, soil permeability and ASMC. Many studies have been performed in order to derive empirical relationships and many papers have also compared these formulae, also showing that they can provide contradictory results (Grimaldi et al., 2012). In this study, the critical duration of rainfall of the CIA formula was calculated according to two empirical relationships, which are usually applied for small basins, thus, both are in agreement with the limited extension of the considered hillslope (around 0.1 Km^2). They are the well-known

530 Kirpich formula (Kirpich, 1940), $t_{cr}^{(1)}$, and that developed by the USA Department of Public Works
531 (1995), $t_{cr}^{(2)}$:
532
533 $$t_{cr}^{(1)} = 0.01947 \frac{L^{0.77}}{S_0^{0.385}} \quad (29)$$
534
535 where the L(m) is the main length of the hillslope, and
536
537 $$t_{cr}^{(2)} = 60\left(11.9 \frac{L^3}{H}\right)^{0.385} \quad (30)$$
538
539 where the maximum distance between the watershed divide and the outlet, L, is in miles, whereas
540 the maximum elevation difference between the watershed divide and the outlet, H, is in feet. Both
541 $t_{cr}^{(1)}$ and $t_{cr}^{(2)}$ are in minutes. Results of the applications of Eq. (29) and Eq. (30) gave very similar
542 results, 4.3 and 4.31 min, which corresponds to a critical rainfall intensity, i_{cr} = 391 mm/h. This was
543 to be expected because both are limited to very small basin areas.
544 The application of the CIA formula also requires the hard estimation of the runoff
545 coefficient, C, which, as observed in section 1, probably represents the crucial point of the
546 hydrologic study. C could be estimated by using one of the available runoff coefficient tables,
547 which however are often based on a qualitative hillslope description. As for the critical rainfall
548 duration, two procedures, i.e. runoff coefficient tables, were selected for the C coefficient
549 estimation. According to the limited hydraulic conductivity (K_s = 0.72 mm/h) and the slope value
550 (greater than 7%), and the selected return period, runoff coefficient values reported in Chow et al.
551 (1988) and in NRCS USDA (1986) provide C values around 0.4-0.44. Similar values could be
552 obtained if referring to the descriptive characteristics of the four SCS soil groups. These C values
553 correspond to a peak discharge more than twice (4-4.45 m^3/s) that determined according to the

554 suggested procedure (2.02 m^3/s), which is likely due to the very high rainfall intensity obtained for
555 the two t_{cr} formulations considered for the CIA formula (Eq. 29 and Eq. 30). A lower suitable value
556 was indeed obtained for the suggested procedure (i_{cr} = 118.3 mm/h, **Table 2**).

557 Of course, the different results do not allow us to conclude that the suggested procedure
558 provides more reliable results than the classical CIA formula, since very simplifying hypotheses are
559 assumed in both procedures. However, the suggested procedure, which is also affected by the
560 assumption of the Green-Ampt and kinematic wave models, could be use in place or together with
561 the classical tables they need, which are usually derived on empirical bases and for this reason can
562 be applied only when strictly hydrological similitudes with the conditions for their derivations are
563 established. On the contrary, the suggested procedure is physically based and so is not affected by
564 subjectivity, since it does not depends on arbitrary evaluations of the factors influencing the
565 estimation of the runoff coefficient, the critical duration of rainfall and thus the peak discharge.

566

567 **5. Conclusions**

568

569 In order to theoretically derive an advanced rational formula giving a "rational" runoff
570 coefficient, *C*, and the peak discharge, q_{cr}, a number of assumptions have been made. These
571 assumptions, some of which are mentioned (homogenous and isotropy of the soil, planar hillslope,
572 uniform AMSC profile, etc.) are linked to the three simplified and more or less consolidated models
573 that were combined: (i) the Green-Ampt model (GA) to account for the infiltration, (ii) the
574 kinematic wave model (KW) to account for the rainfall excess transportation, and (iii) the intensity-
575 duration-frequency curves (IDF) to describe the maximum rainfall intensity, for fixed return period,
576 *T*.

577 This procedure strongly differs from empirical ones, since it leads to physically based runoff
578 coefficients that are not affected by personal evaluations, on the basis of parameters with a clear
579 physical meaning, describing rainfall, hillslope geometry and soil. Thus, most of the limits of the

rational formula were removed (i.e. linearity of the hillslope response, subjectivity in *C* estimation, *C* time independence and return period independence, subjectivity in the estimation of the critical duration of rainfall, neglecting time to ponding).

Differently from the past, it is shown that this kind of approach leads to arranging rational runoff coefficient tables where no qualitative descriptions need to be fixed. These tables reproduce the physically based solutions of the mentioned approach, where the characteristics of rainfall, soil and hillslope geometry are set according to parameters of clear physical meaning. Thus, they can be used for a revisited rational method in place of the classical tables that are usually derived on empirical bases and for this reason can be applied only when strictly hydrological similitudes with the conditions for their derivations are established.

Although the work is directed towards deriving the peak discharge at the hillslope scale for a fixed rainfall structure parameter, *n*, it could be also apply for different *n* values, in order to detect its influence on the peak discharge estimation. This latter issue was only addressed for saturated soil condition. Moreover, following this line of thinking, this approach may even open doors for deriving peak discharge for hill slopes with a complex topography for which, solutions were already obtained under impervious hill slope conditions. Finally, it seems to be promising to also consider the network response contribute and complex design hyetograph, which could be advisable especially for rainfall with a long critical duration, which were not considered in this work.

References

Agnese, C., V. Bagarello, G. Baiamonte, and M. Iovino, (2011), Comparing physical quality of forest and pasture soils in a sicilian watershed, *Soil Sci. Soc. Am. J.*, 75, 1958-1970.

Agnese, C., G. Baiamonte, and C. Cammalleri (2014), Modelling the occurrence of rainy days under a typical Mediterranean climate, *Adv. Water Resour.*, 64, 62-76, http://dx.doi.org/10.1016/j.advwatres.2013.12.005.

606 Agnese, C., G. Baiamonte, and C. Corrao (2001), A simple model of hillslope response for overland
607 flow generation, *Hydrol Process*, 15, 3225-3238, ISSN: 0885-6087, doi: 10.1002/hyp.182.
608 Agnese, C., G. Baiamonte, and C. Corrao (2007), Overland flow generation on hillslopes of
609 complex topography: Analytical Solutions, *Hydrol Process,* 21(10):1308-1317, doi:
610 10.1002/hyp.6354.
611 Agnese, C., G. Baiamonte, F. D'Asaro, and G. Grillone (2016), Probability Distribution of Peak
612 Discharge at the Hillslope Scale Generated by Hortonian Runoff, *J. Irrig. Drain. E-ASCE*,
613 142(2), 10.1061/(ASCE)IR.1943-4774.0000973, 04015052.
614 Baiamonte, G. (2016), A simplified model to predict runoff generation time for well-drained and
615 vegetated soils, *J. Irrig. Drain. E-ASCE,* doi: 10.1061/(ASCE)IR.1943-4774.0001072.
616 Baiamonte, G., and C. Agnese (2010), An analytical solution of kinematic wave equations for
617 overland flow under Green-Ampt infiltration, *J. Agr. Eng.*, vol. 1, p. 41-49, ISSN: 1974-7071.
618 Baiamonte, G., and C. Agnese (2016), Quick and Slow Components of the Hydrologic Response at
619 the Hillslope Scale, *J. Irrig. Drain.* E-ASCE, 142(10), doi: 10.1061/(ASCE)IR.1943-
620 4774.0001053, 04016038.
621 Baiamonte, G., V. Bagarello, F. D'Asaro, F., and V. Palmeri (2017), Factors influencing point
622 measurement of near-surface saturated soil hydraulic conductivity in a small Sicilian basin,
623 *Land Degradation and Development*, doi: 10.1002/ldr.2674.
624 Baiamonte, G., and F. D'Asaro (2016), Discussion of "Analysis of Extreme Rainfall Trends in
625 Sicily for the Evaluation of Depth-Duration-Frequency Curves in Climate Change Scenarios"
626 by Lorena Liuzzo and Gabriele Freni." *J Hydrol E-ASCE*. doi: 10.1061/(ASCE)HE.1943-
627 5584.0001381, 07016005.
628 Baiamonte, G., F. D'Asaro, and G. Grillone (2014), Simplified probabilistic-topologic model for
629 reproducing hillslope rill network surface runoff, *J. Irrig. Drain. Eng.*,
630 10.1061/(ASCE)IR.1943-4774.0000854 , 04014080.

631 Baiamonte, G., and V.P. Singh (2016a), Analytical Solutions of Kinematic Wave Time of
632 Concentration for Overland Flow under Green-Ampt Infiltration, *J. Hydrol. E* – ASCE, 21(3),
633 doi: 10.1061/(ASCE)HE.1943-5584.0001266, 04015072.
634 Baiamonte, G., and V.P. Singh (2016b), Overland Flow Times of Concentration for Hillslopes of
635 Complex Topography, *J. Irrig. Drain.* E-ASCE, 142(3), doi: 10.1061/(ASCE)IR.1943-
636 4774.0000984, 04015059.
637 Bedient, P.B., and W.C. Huber (1988), Hydrology and Floodplain Analysis. Addison-Wesley
638 Publishing Company, pp. 360-364.
639 Blöschl, G., M. Sivapalan, T. Wagener, A. Viglione, and H. Savenije (2013), Runoff Prediction in
640 Ungauged Basins: Synthesis across Processes, Places and Scales, CAMBRIDGE University
641 Press, 484 pages | Hardback 1st edition | April 2013, ISBN 978-1-107-02818-0.
642 Chen, C.N., and T.S.W. Wong (1993), Critical Rainfall Duration for Maximum Discharge from
643 Overland Plane, Journal of Hydraulic Engineering 119(9), DOI: 10.1061/(ASCE)0733-
644 9429(1993)119:9(1040).
645 Chin, D. (2013). Water-resources engineering, 3rd Ed., Pearson, Upper Saddle River, NJ.
646 Chin, D. (2017). Discussion of "Return Period–Dependent Rational Formula Coefficients for Two
647 Locations in Texas" by David C. Froehlich, J. Irrig. Drain Eng., 2017, 143(9): 07017014
648 Chow, V.T., D. R. Maidment, and L.W. Mays (1988), Applied hydrology, McGraw Hill, New
649 York.
650 Cundy, T.W., and S.W. Tento (1985), Solution to the kinematic wave approach to overland flow
651 routing with rainfall excess given by Philip's equation, Water Resour. Res., 21, 1132-1140.
652 Cullotta, S., V. Bagarello, G. Baiamonte, G. Gugliuzza, M. Iovino, D.S. La Mela Veca, F. Maetzke,
653 V. Palmeri and S. Sferlazza (2016), Comparing different methods to determine soil physical
654 quality in a Mediterranean forest and pasture land", Soil Science Society of America Journal,
655 Doi: 10.2136/sssaj2015.12.0447.

656 de Almeida, I.K., A.K. Almeida, J.A.A. Anache, J.L. Steffen, and T, Alves Sobrinho (2016), Model
657 for estimating the time of concentration in watersheds. Water Resources Management, 30
658 (12), 4083–4096. doi:10.1007/s11269-016-1383-x.
659 Dhakal, N., X. Fang, T.G. Cleveland, D.B. Thompson, W.H. Asquith, and L.J. Marzen (2012),
660 Estimation of volumetric runoff coefficients for Texas watersheds using land-use and rainfall–
661 runoff data, Journal of Irrigation and Drainage Engineering, 138, 43–
662 54.10.1061/(ASCE)IR.1943-4774.0000368
663 Dhakal, N., X. Fang, W.H. Asquith, T.G. Cleveland, and D.B. Thompson (2013), Return period
664 adjustment for runoff coefficients based on analysis in undeveloped Texas watersheds,
665 Journal of Irrigation and Drainage Engineering, 139 (6), 476–482. 10.1061/(ASCE)IR.1943-
666 4774.0000571.
667 Department of Public Works (1995), California culvert practice, second edition. Sacramento, CA:
668 DPW, Division of Highways.
669 Froehlich, D.C. (2016), Return Period–Dependent Rational Formula Coefficients for Two Locations
670 in Texas, J. Irrig. Drain Eng.ASCE, 142(9): 04016035, pp. 1-12.
671 Haktanir, T., and N. Sezen (1990), Suitability of two-parameter gamma and three-parameter beta
672 distributions as synthetic unit hydrographs in Anatolia. Hydrol. Sci. J., 35(2), 167–184.
673 Johnstone, D., and W.P. Cross (1949), Elements of applied hydrology, Ronald Press, New York.
674 Green W.H., and G.A. Ampt, (1911), Studies of soil physics, I, Flow of air and water through soils,
675 Journal of Agricultural Science, 4:1-24.
676 Grimaldi, S., Petroselli A., Tauro F., and M. Porfiri (2012). Time of concentration: A paradox in
677 modern hydrology. Hydrological Sciences Journal, 57 (2), 217–228.
678 Grimaldi, S., and A. Petroselli (2015), Do we still need the Rational Formula? An alternative
679 empirical procedure for peak discharge estimation in small and ungauged basins,
680 Hydrological Sciences Journal, DOI: 10.1080/02626667.2014.880546.

681 Kirpich, Z.P. (1940), Time of concentration of small agricultural watersheds, Civ. Eng. (N.Y.),
682 10(6), 362.
683 Morel-Seytoux, H., and J. Verdin (1981), Extension of soil conservation service rainfall runoff
684 methodology for ungaged watersheds. Rep. FHWA/RD-81/060, Federal Highway
685 Administration,Washington, DC.
686 Mulvaney, T.J. (1851), On the use of self-registering rain and flood gauges in making observations
687 of the relations of rainfall and flood discharges in a given catchment. Proceedings of the
688 Institution of Civil Engineers of Ireland, 4, 19–31.
689 Ostrowski, M.W. (2003), Linearity of hydrological models and related uncertainty. Proceedings of
690 the ESF LESC Exploratory Workshop on "Hydrological Risk: recent advances in peak river
691 flow modelling, prediction and real-time forecasting. Assessment of the impacts of land-use
692 and climate changes", Bologna, Italy, October 24-25.
693 Papanicolaou, A.P., M. Elhakeem, C.G. Wilson, C.L. Burras, L.T. West, H. Lin, B. Clark, and B.E.
694 Oneal (2015), Spatial variability of saturated hydraulic conductivity at the hillslope scale:
695 Understanding the role of land management and erosional effect, *Geoderma*, 243–244, 58–68,
696 doi.org/10.1016/j.geoderma.2014.12.010.
697 Robinson J.S., M., Sivapalan, and J.D. Snell (1995), On the relative roles of hillslope processes,
698 channel routing, and network geomorphology in the hydrologic response of natural
699 catchment, Water Resour. Res., 31, 3089-3101.
700 Simas, M.J., and R.H. Hawkins (2002), Lag time characteristics in small watersheds in the United
701 States, Proc., 2nd Federal Interagency Hydrologic Modeling Conf., Las Vegas.
702 Sivapalan, M. (2003), Prediction in ungauged basins: a grand challenge for theoretical hydrology,
703 Hydrol. Process. 17, 3163–3170.
704 Tay H.N., and N.R. Afshar (2014), Evaluation of runoff coefficient (Samarahan Basin).
705 International Engineering Conference, Energy and Environment (ENCON 2014) Copyright ©

2014 Editor(s), ENCON 2014. Published by Research Publishing. ISBN: 978-981-09-4587-9, doi: 10.3850/978-981-09-4587-9_P19.

Thompson, D.B. (2006), The rational method, Regional regression equations, and site-specific flood-frequency relations, Report No. 0-4405-I, Texas Department of Transportation Research and Technology, Austin, TX 78763-5080.

United States Department of Agriculture, Natural Resources Conservation Service (1986). Urban Hydrology for Small Watersheds, 210-VI-TR-55, Second Ed., June.

U.S. Environmental Protection Agency (USEPA) (1983), "Results of the nationwide urban runoff program: Vol. 1—Final report." National Technical Information Service (NTIS) Accession No. PB84-185552, Water Planning Division, Washington, DC.

Viessman, W., and G.L. Lewis (2003), Introduction to hydrology, 5th Ed., Pearson Education, Upper Saddle River, NJ, 612.

Wijesinghe W.M.D., and N.T.S. Wijesekera (2011), Comparison of Rational Formula Alternatives for Streamflow Generation for Small Ungauged Catchments. ENGINEER - Vol. XXXXIV, No. 04, pp. 28-35, © The Institution of Engineers, Sri Lanka.

Williams, G.B. (1922), Flood discharges and the dimensions of spillways in India. Engineering (London), 134, 321.

Woolhiser, D.A., and J.A. Liggett (1967), Unsteady one-dimensional flow over a plane-The rising hydrograph." Water Resour. Res., 3(3), 753–771.

Figure_1.

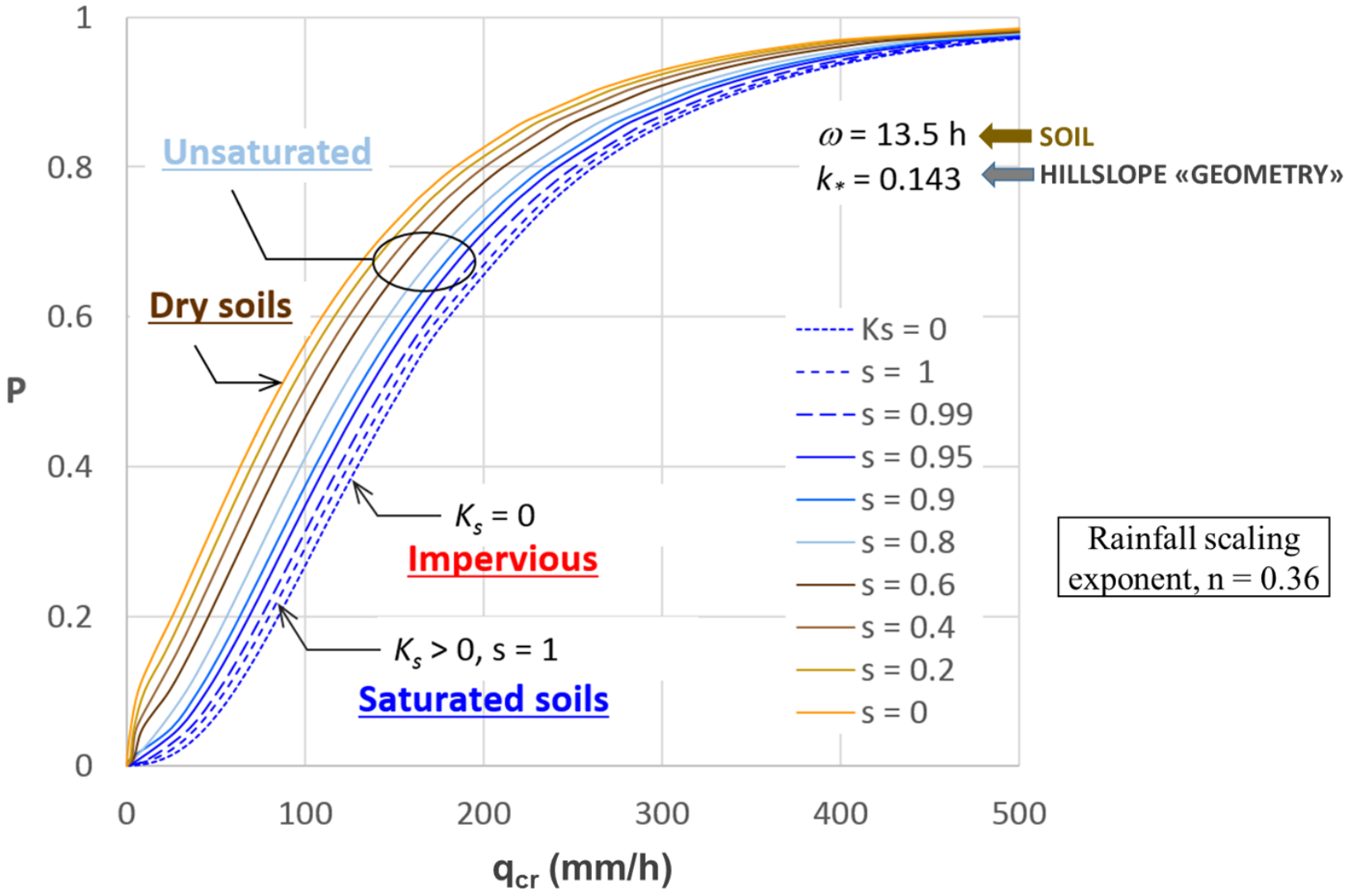
1
0.8
0.6
0.4
0.2
0
P
0
100
200
300
400
500
q_{cr} (mm/h)
Unsaturated
Dry soils
K_s = 0
Impervious
K_s > 0, s = 1
Saturated soils
ω = 13.5 h
SOIL
k_* = 0.143
HILLSLOPE «GEOMETRY»
Ks = 0
s = 1
s = 0.99
s = 0.95
s = 0.9
s = 0.8
s = 0.6
s = 0.4
s = 0.2
s = 0
Rainfall scaling exponent, n = 0.36

Figure 2ab.

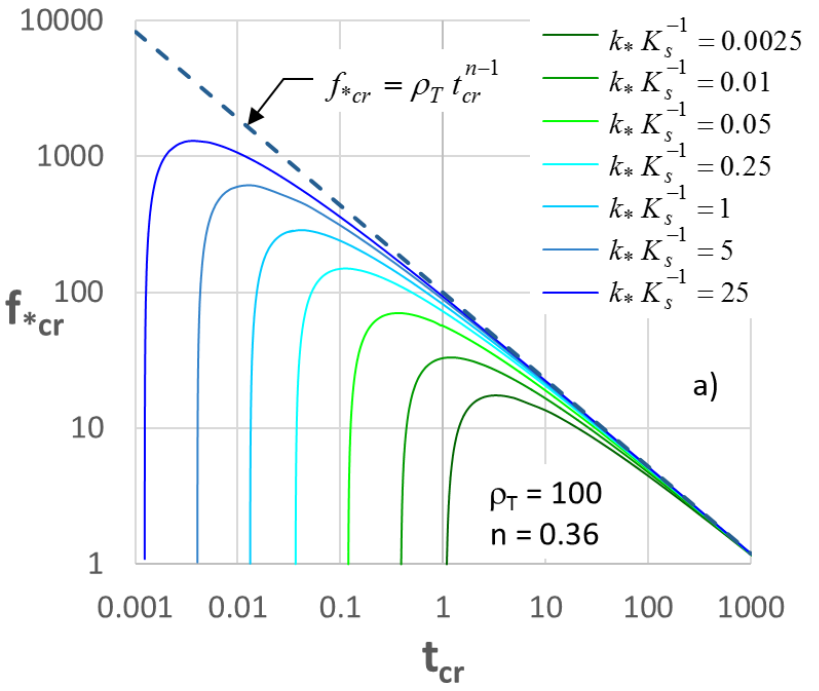
10000
1000
100
10
1
f_{*cr}
0.001
0.01
0.1
1
10
100
1000
t_{cr}
$f_{*cr} = \rho_T \, t_{cr}^{n-1}$
$k_* K_s^{-1} = 0.0025$
$k_* K_s^{-1} = 0.01$
$k_* K_s^{-1} = 0.05$
$k_* K_s^{-1} = 0.25$
$k_* K_s^{-1} = 1$
$k_* K_s^{-1} = 5$
$k_* K_s^{-1} = 25$
a)
ρ_T = 100
n = 0.36

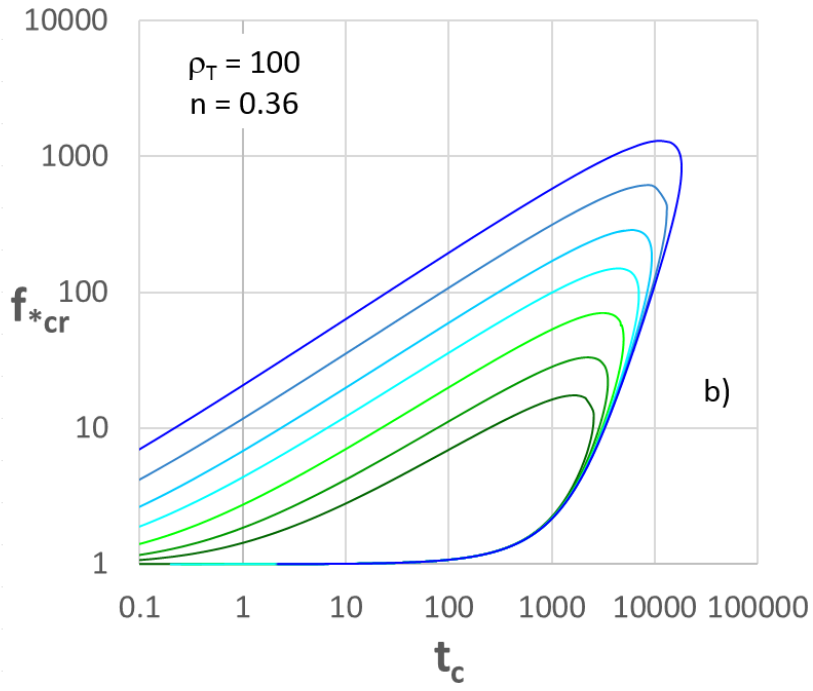
10000
1000
100
10
1
f_{*cr}
0.1
1
10
100
1000
10000
100000
t_c
ρ_T = 100
n = 0.36
b)

Figure 3ab.

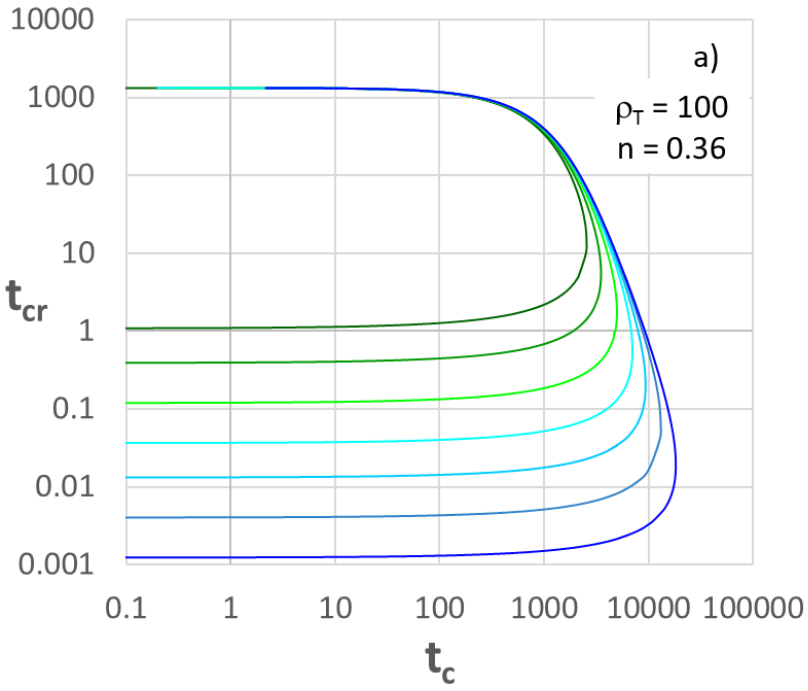
a)
ρ_T = 100
n = 0.36
t_{cr}
t_c
10000
1000
100
10
1
0.1
0.01
0.001
0.1
1
10
100
1000
10000
100000

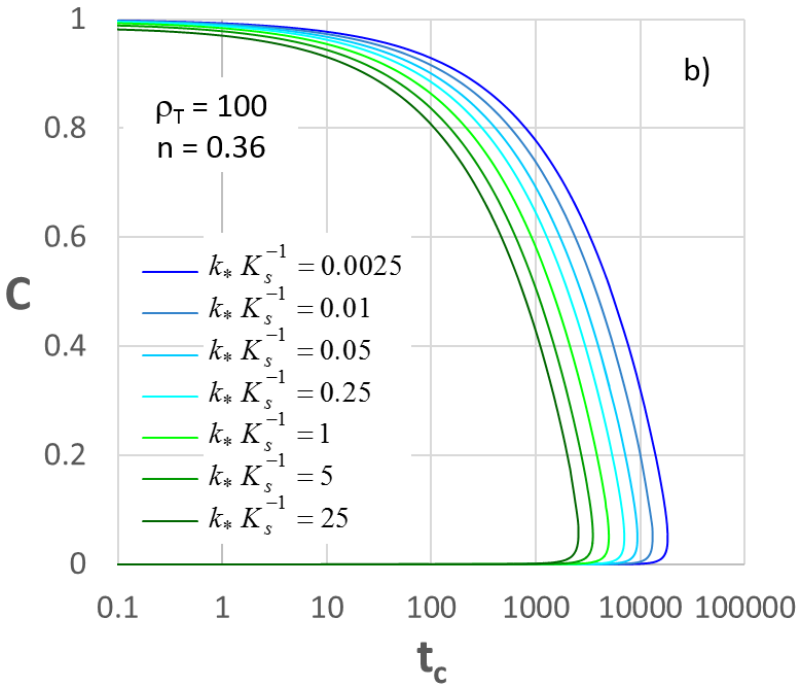
b)
ρ_T = 100
n = 0.36
C
t_c
$k_* K_s^{-1} = 0.0025$
$k_* K_s^{-1} = 0.01$
$k_* K_s^{-1} = 0.05$
$k_* K_s^{-1} = 0.25$
$k_* K_s^{-1} = 1$
$k_* K_s^{-1} = 5$
$k_* K_s^{-1} = 25$
1
0.8
0.6
0.4
0.2
0
0.1
1
10
100
1000
10000
100000

Figure 4ab.

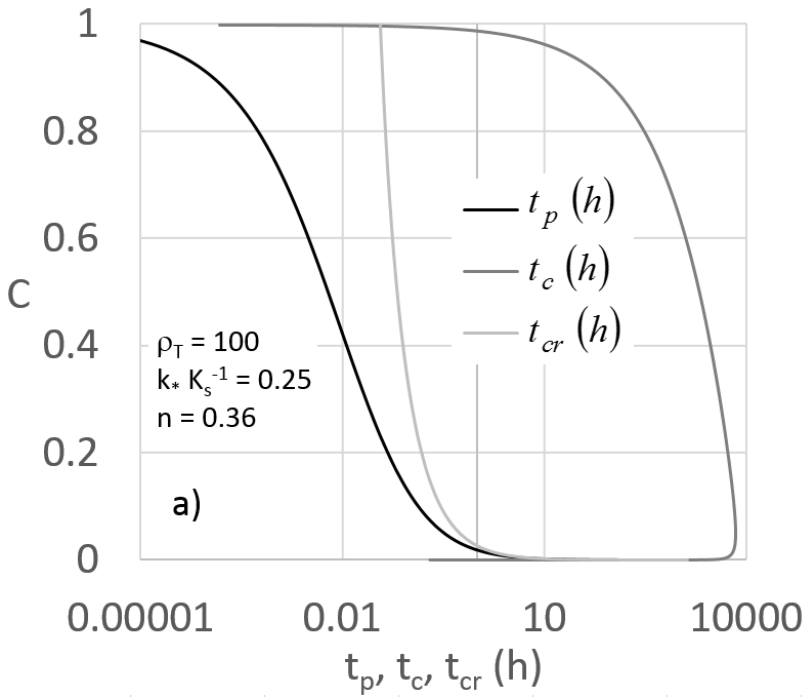
1
0.8
0.6
0.4
0.2
0
C
$t_p\ (h)$
$t_c\ (h)$
$t_{cr}\ (h)$
ρ_T = 100
$k_* K_s^{-1}$ = 0.25
n = 0.36
a)
0.00001
0.01
10
10000
t_p, t_c, t_{cr} (h)

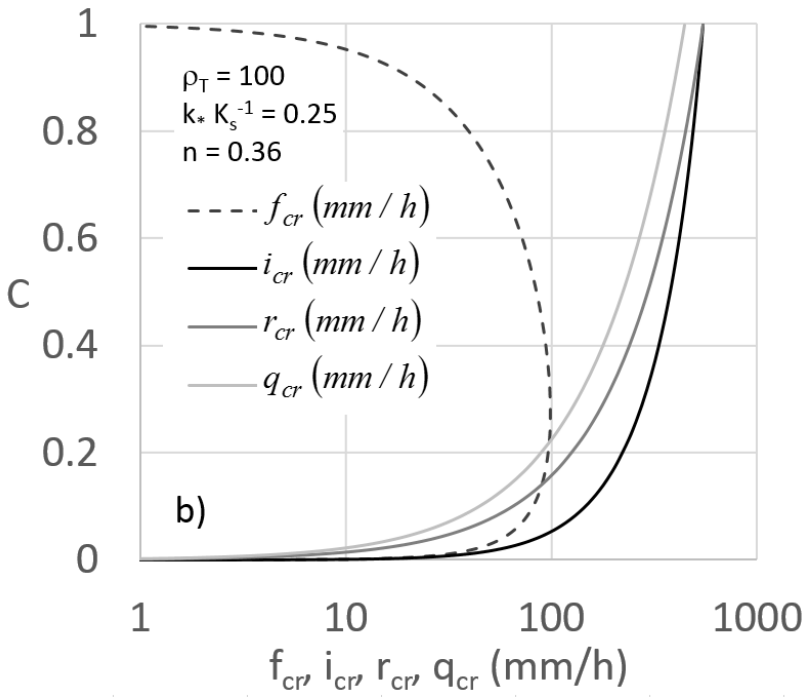
1
0.8
0.6
0.4
0.2
0
C
ρ_T = 100
$k_* K_s^{-1}$ = 0.25
n = 0.36
$f_{cr}\ (mm/h)$
$i_{cr}\ (mm/h)$
$r_{cr}\ (mm/h)$
$q_{cr}\ (mm/h)$
b)
1
10
100
1000
f_{cr}, i_{cr}, r_{cr}, q_{cr} (mm/h)

Figure 5ab.

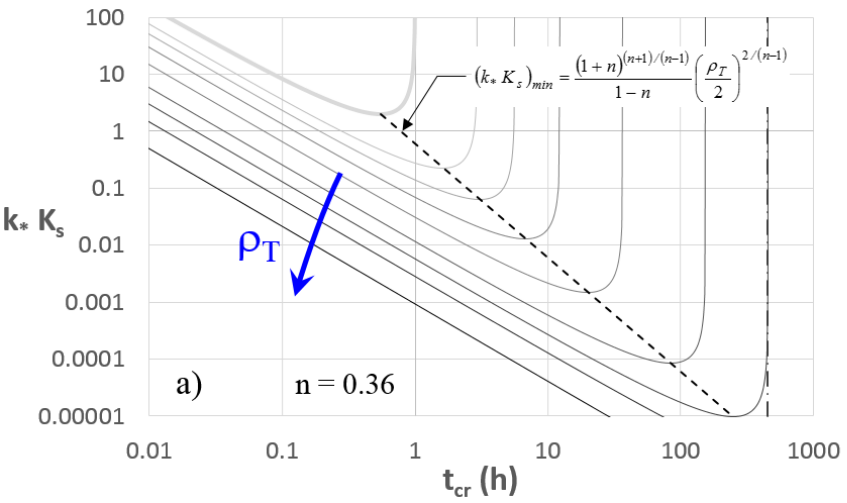
100
10
1
0.1
0.01
0.001
0.0001
0.00001
k* Ks
0.01
0.1
1
10
100
1000
tcr (h)
$(k_* K_s)_{min} = \frac{(1+n)^{(n+1)/(n-1)}}{1-n}\left(\frac{\rho_T}{2}\right)^{2/(n-1)}$
ρT
a)
n = 0.36

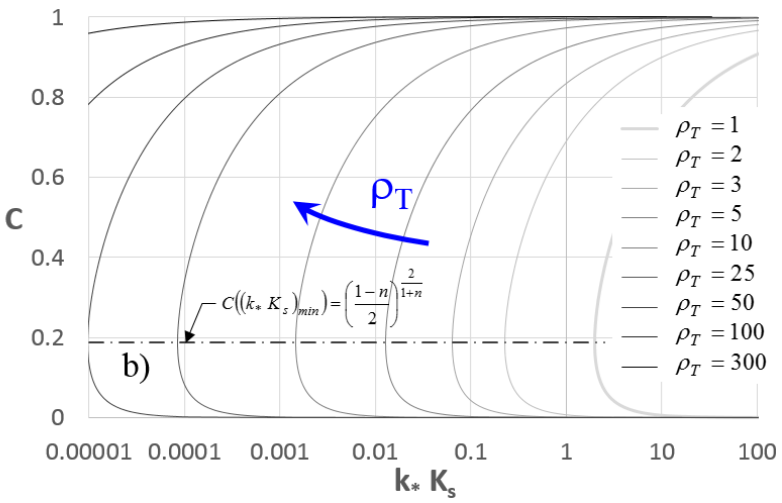
1
0.8
0.6
0.4
0.2
0
C
0.00001
0.0001
0.001
0.01
0.1
1
10
100
k* Ks
$C((k_* K_s)_{min}) = \left(\frac{1-n}{2}\right)^{\frac{2}{1+n}}$
ρT
b)
$\rho_T = 1$
$\rho_T = 2$
$\rho_T = 3$
$\rho_T = 5$
$\rho_T = 10$
$\rho_T = 25$
$\rho_T = 50$
$\rho_T = 100$
$\rho_T = 300$

Figure 6a.

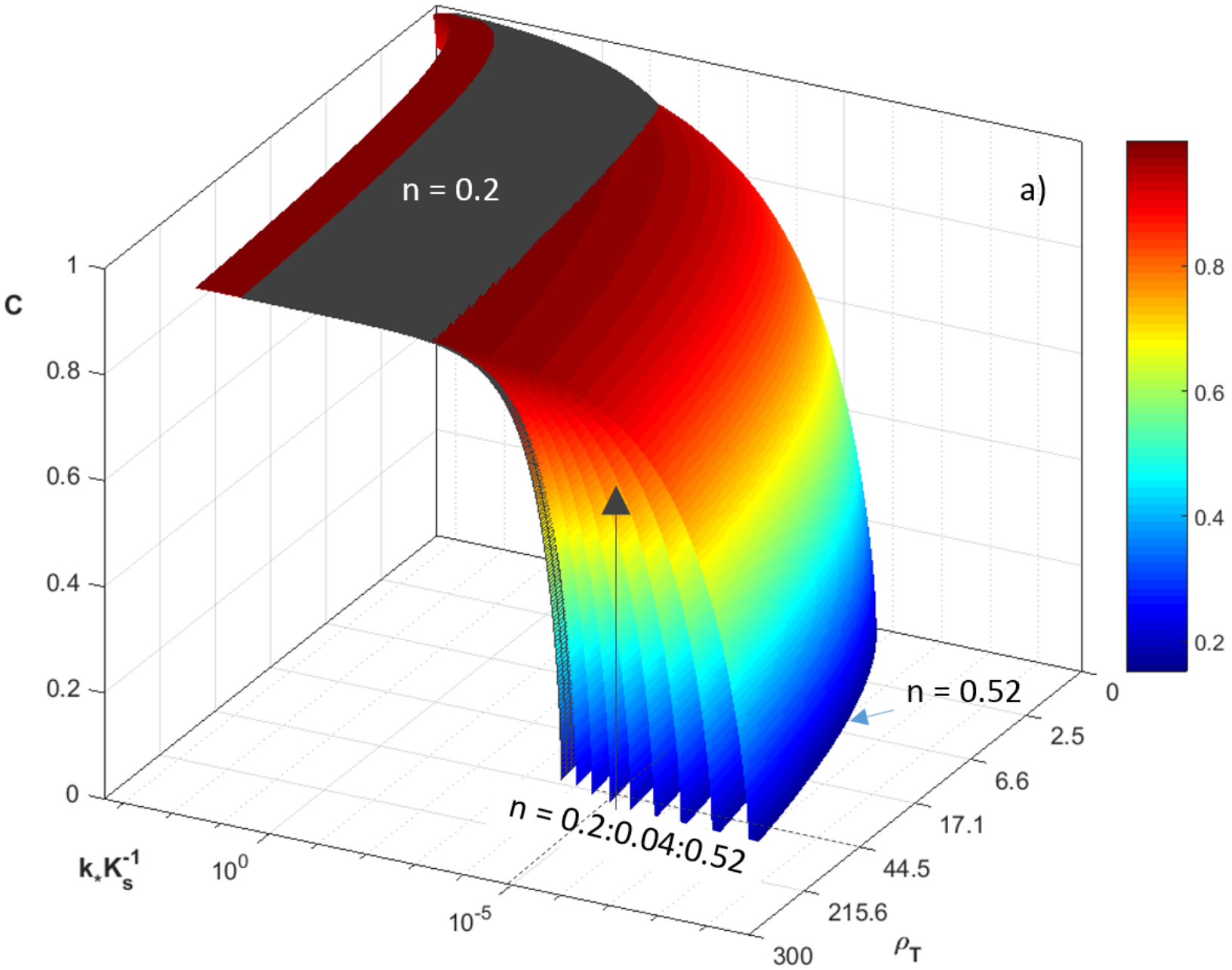
n = 0.2
a)
C
1
0.8
0.6
0.4
0.2
0
$k_* K_s^{-1}$
10^0
10^{-5}
n = 0.2:0.04:0.52
n = 0.52
0
2.5
6.6
17.1
44.5
215.6
300
ρ_T
0.8
0.6
0.4
0.2

Figure 6b.

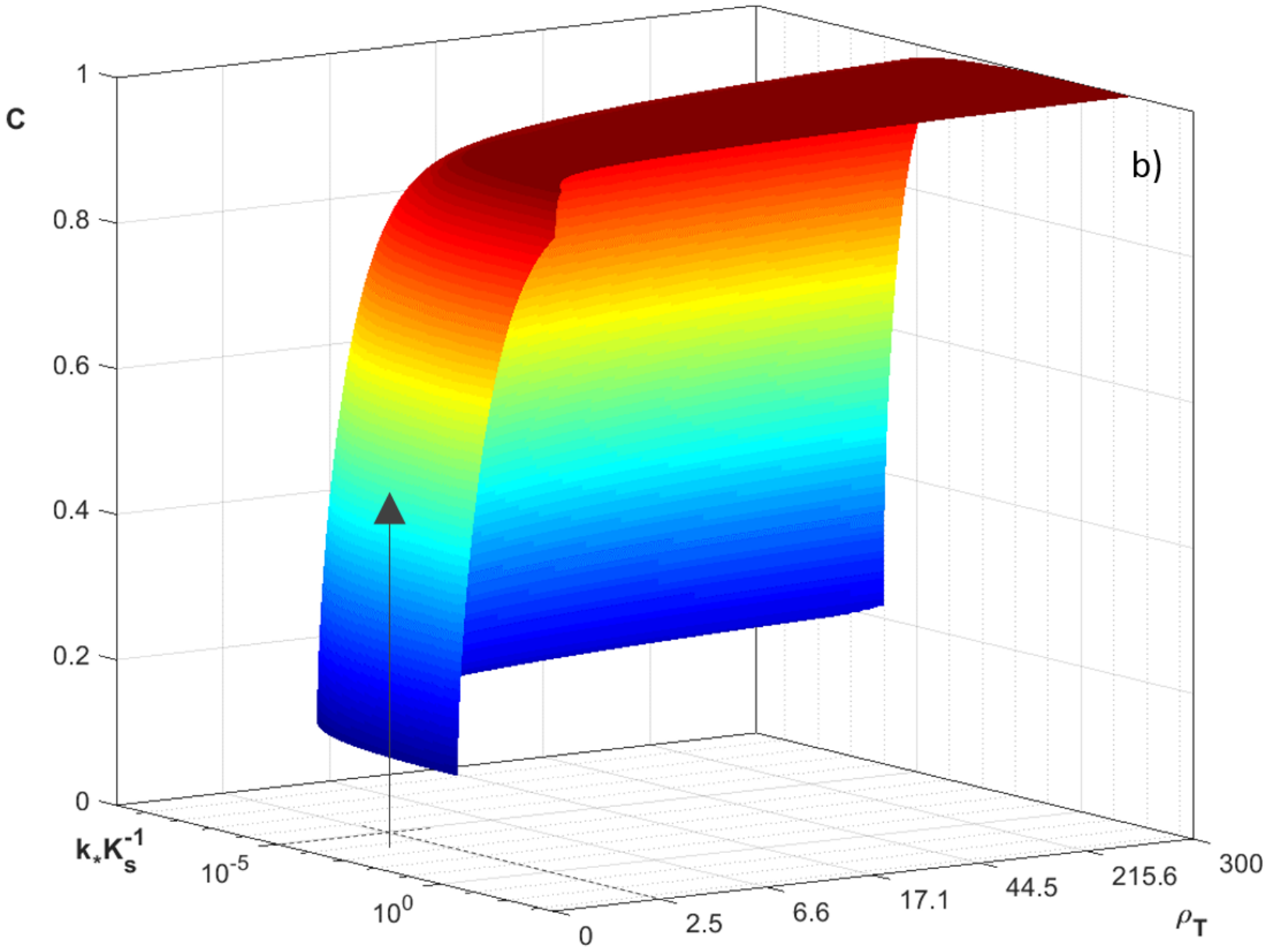
c
1
0.8
0.6
0.4
0.2
0
b)
$k_* K_s^{-1}$
10^{-5}
10^{0}
0
2.5
6.6
17.1
44.5
215.6
300
ρ_T

Figure 7.

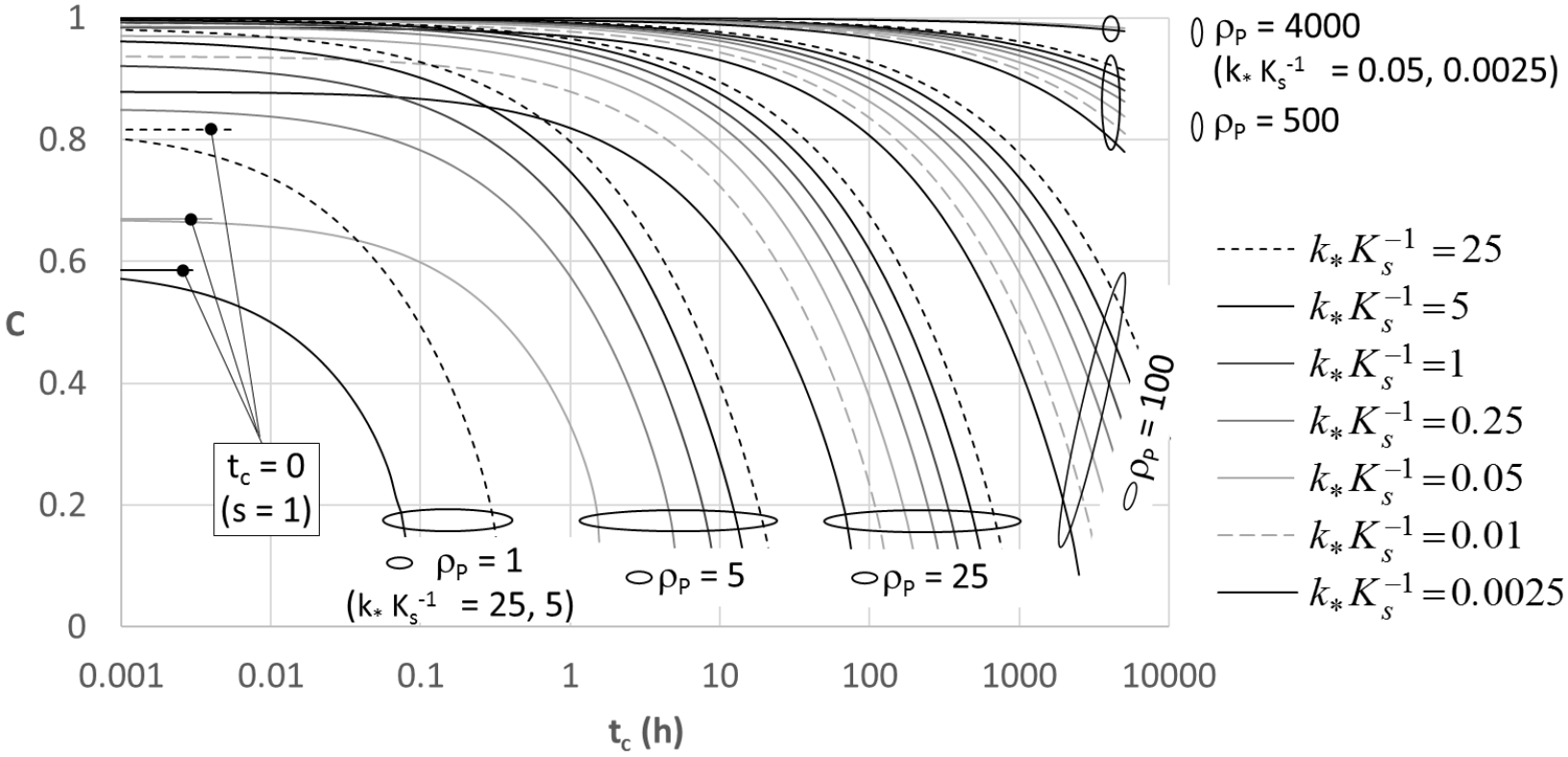
1
0.8
0.6
0.4
0.2
0
c
0.001
0.01
0.1
1
10
100
1000
10000
t_c (h)
t_c = 0
(s = 1)
ρP = 1
(k* Ks^-1 = 25, 5)
ρP = 5
ρP = 25
ρP = 100
ρP = 4000
(k* Ks^-1 = 0.05, 0.0025)
ρP = 500
k*Ks^-1 = 25
k*Ks^-1 = 5
k*Ks^-1 = 1
k*Ks^-1 = 0.25
k*Ks^-1 = 0.05
k*Ks^-1 = 0.01
k*Ks^-1 = 0.0025

Figure 8.

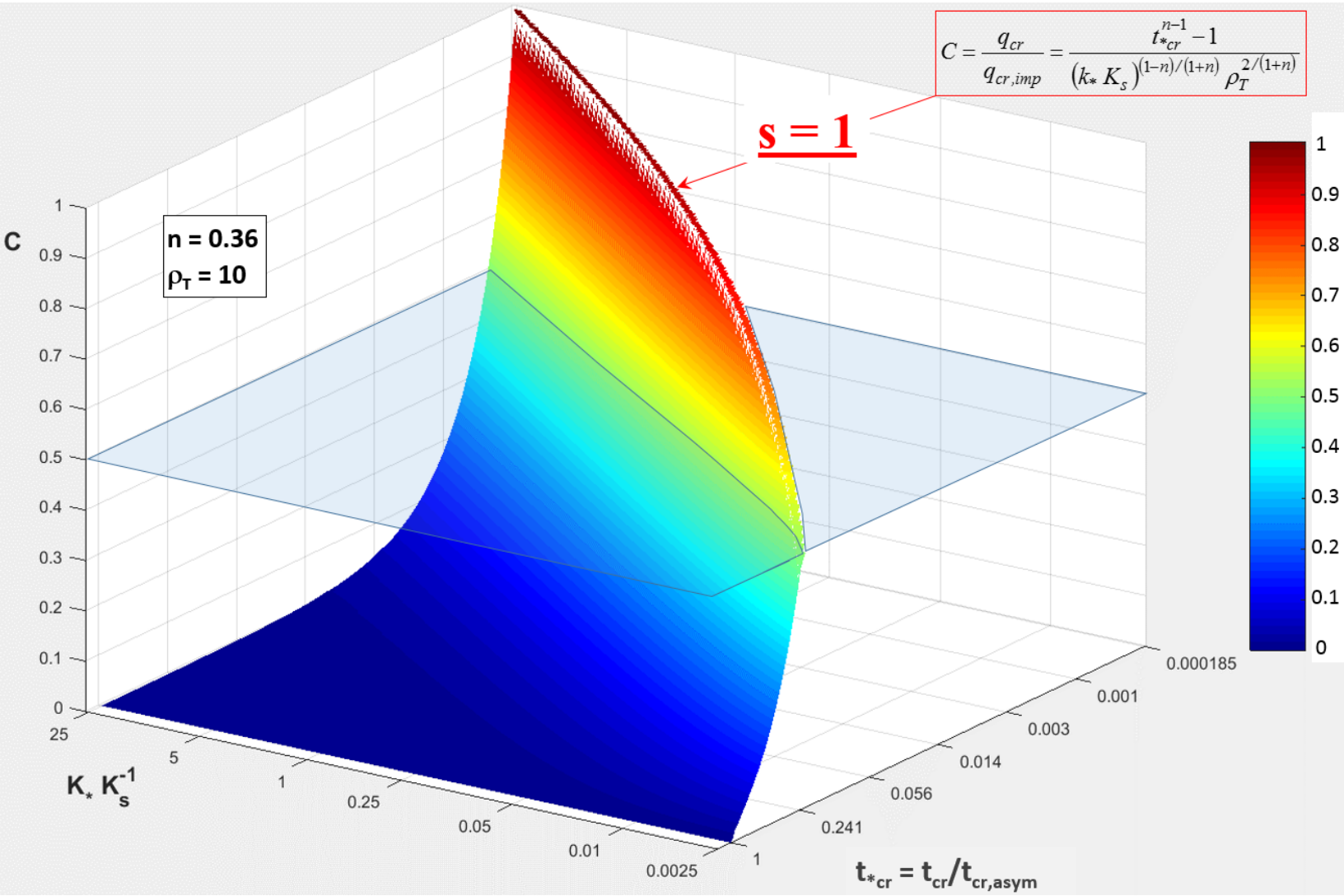
$C = \frac{q_{cr}}{q_{cr,imp}} = \frac{t_{*cr}^{n-1} - 1}{(k_* K_s)^{(1-n)/(1+n)} \rho_T^{2/(1+n)}}$
s = 1
n = 0.36
ρ_T = 10
C
1
0.9
0.8
0.7
0.6
0.5
0.4
0.3
0.2
0.1
0
25
5
1
0.25
0.05
0.01
0.0025
$K_* K_s^{-1}$
1
0.241
0.056
0.014
0.003
0.001
0.000185
$t_{*cr} = t_{cr}/t_{cr,asym}$

Figure 9.

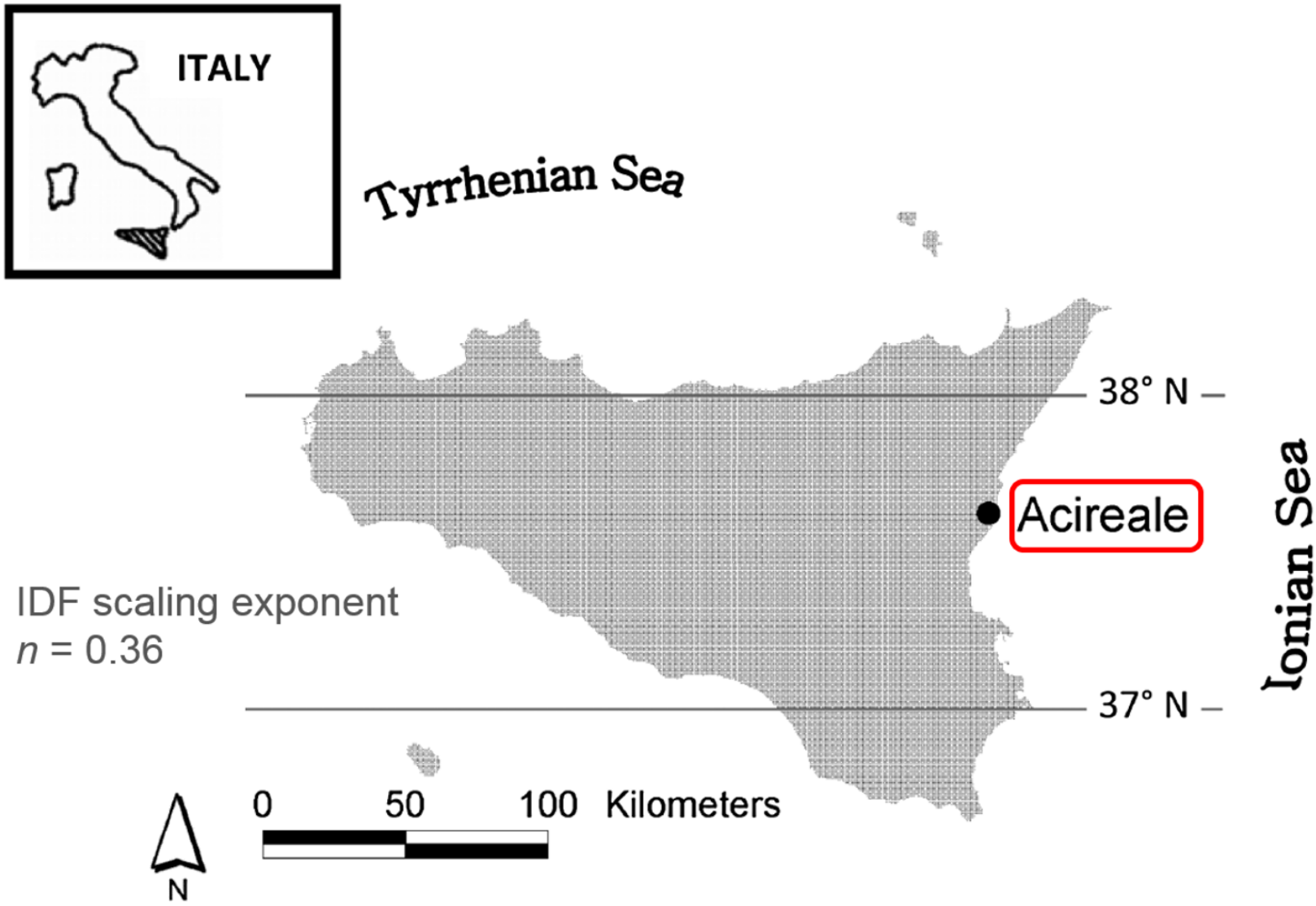
ITALY
Tyrrhenian Sea
38° N
Acireale
37° N
Ionian Sea
IDF scaling exponent
n = 0.36
0
50
100
Kilometers
N

FIGURE CAPTIONS

Fig. 1 – For ω = 13.5 h, k_* = 0.143, n = 0.36, for impervious hillslopes (K_s = 0) and for different ASMC, s, probability distributions of the peak discharges, q_{cr}, according to the GABS model (Baiamonte and Singh, 2017).

Fig. 2 – For ρ_T = 100 and n = 0.36, relationships between f_{*cr} and a) the critical duration of rainfall, t_{cr}, and b) the sorptivity time scale, t_c, with $k_*K_s^{-1}$ as a parameter. The limiting condition of f_{*cr} at increasing t_{cr} (dashed line) is also represented (Fig. 2a)

Fig. 3 – For ρ_T = 100 and n = 0.36, relationships between a) the critical duration of rainfall, t_{cr}, and b) the runoff coefficient, C, versus the sorptivity time scale, t_c, with $k_*K_s^{-1}$ as a parameter.

Fig. 4 – For ρ_T = 100, $k_*K_s^{-1}$ = 0.25 and n = 0.36, relationships between the runoff coefficient, C, a) and the time dimension variables, t_p (Eq, 3), t_c (Eq, 4) and t_{cr} (Eq, 9), and b) versus the flux dimension variable, f_{cr} (Eq, 9), i_{cr} (Eq, 7), r_{cr} and q_{cr} (Eq, 13).

Fig. 5 – For saturated soil conditions (t_c = 0, s = 1), relationships a) between k_*K_s parameter and the critical duration of rainfall, t_{cr}, and b) between the runoff coefficient, C, and k_*K_s parameter, for different ρ_T values. The minimum value of k_*K_s, $(k_*K_s)_{min}$ (Eq. 20), and the corresponding C value, $C((k_*K_s)_{min})$, are represented (Fig. 5a and Fig. 5b, respectively).

Fig. 6 – For saturated soil conditions (t_c = 0, s = 1), two different 3D views, a) and b), of the runoff coefficient, C, versus $k_*K_s^{-1}$ and versus ρ_T parameters, for different values of the rainfall structure parameter, n. For a fixed $k_*K_s^{-1} = 10^{-5}$, the arrow illustrates the n-dependence and the n-independence of C a) for a high ρ_T = 44.5 and b) for a low ρ_T = 2.5, respectively.

Fig. 7 – Runoff coefficient, C (Eq. 11), versus the sorptivity time scale, t_c, for different $k_*K_s^{-1}$ and ρ_T values. Ovals group the $C(t_c)$ relationships for fixed ρ_T. For ρ_T = 1 ($k_*K_s^{-1}$ = 25, 5) and for ρ_T = 5 ($k_*K_s^{-1}$ = 25, 0.05), the limiting condition of C for saturated soil conditions (t_c = 0, s = 1, Eq. 22) is also illustrated.

Fig. 8 – For ρ_T = 10 and n = 0.36, 3D plot of the runoff coefficient, C, versus $k_*K_s^{-1}$ and versus the normalized critical duration of rainfall, t_{*cr}, according to Eq. (24). The runoff coefficient, C, corresponding to the saturated soil conditions (t_c = 0, s = 1, Eq. 26) as the limiting condition of the general C solution (Eq. 24) is also illustrated.

Fig. 9 – Location of Acireale raingauge, in the Sicilian Region, for which the maximum hourly rainfall intensity data-series of the Acireale station (Sicily), with a high sample size (N = 60), was considered in the application (Table 2).

Table 1 – Runoff coefficient table, for rainfall structure parameter, n = 0.36. Bold values in brackets are the C coefficient corresponding to saturated soil conditions (t_c = 0, s = 1, Eq. 26).

$k_* K_s^{-1}$	C	t_c (h)								
		ρ_T = 1	ρ_T = 2	ρ_T = 3	ρ_T = 5	ρ_T = 10	ρ_T = 25	ρ_T = 50	ρ_T = 100	ρ_T = 300
0.00001	1.0									**(0.958)**
	0.9									52
	0.8								**(0.784)**	312
	0.7								14.41	794
	0.6								49.11	1506
	0.5								100.82	2473
	0.4								167.59	3651
	0.3							**(0.252)**	244.78	5095
	0.2							0.38	317.25	6679
	0.1							14.15	340.07	8163
0.0001	1.0								**(0.929)**	**(0.986)**
	0.9								2.88	139
	0.8							**(0.798)**	33.31	624
	0.7							8.13	94.86	1464
	0.6							18.99	189.43	2752
	0.5							37.91	315.93	4360
	0.4						**(0.343)**	62.17	474.16	6437
	0.3						0.33	90.19	661.44	8900
	0.2						1.03	116.74	865.90	11679
	0.1						0.29	126.75	1030.58	14346
0.0005	1.0							**(0.908)**	**(0.967)**	**(0.999)**
	0.9							0.15	12.25	216
	0.8						**(0.733)**	7.80	66.51	923
	0.7						0.45	24.89	167.27	2089
	0.6						3.25	51.63	309.08	3910
	0.5						7.82	87.20	506.56	6297
	0.4						13.84	132.50	747.50	9107
	0.3						20.79	186.34	1037.42	12642
	0.2						26.99	243.49	1359.67	16624
	0.1						27.67	285.02	1653.66	20494
0.0025	1.0							**(0.957)**	**(0.985)**	**(0.997)**
	0.9						**(0.879)**	2.98	23.55	311
	0.8						1.55	18.52	107.49	1255
	0.7						6.07	47.15	254.78	2920
	0.6						13.38	89.57	468.22	5637
	0.5					**(0.480)**	23.48	147.57	750.34	8875
	0.4					0.28	36.23	218.89	1102.68	12934
	0.3					0.77	51.13	304.12	1523.39	17733
	0.2					1.13	66.62	397.95	1998.57	23392
	0.1					0.80	76.32	461.11	2673.40	28976

$k_* K_s^{-1}$	C	t_c (h)								
		$\rho_T = 1$	$\rho_T = 2$	$\rho_T = 3$	$\rho_T = 5$	$\rho_T = 10$	$\rho_T = 25$	$\rho_T = 50$	$\rho_T = 100$	$\rho_T = 300$
0.01	1.0						**(0.938)**	**(0.978)**	**(0.992)**	**(0.998)**
	0.9						0.49	6.06	34.7	464
	0.8					**(0.751)**	4.44	29.44	147.79	1737
	0.7					0.19	12.20	69.95	341	4307
	0.6					0.95	23.89	129.14	632	7555
	0.5					2.14	39.59	210.53	1029	11661
	0.4					3.70	59.26	312.09	1496	17252
	0.3					5.50	82.54	431.21	2076	23778
	0.2					7.15	107.92	564.44	2719	31276
	0.1					7.37	128.74	690.50	3356	38747
0.05	1.0						**(0.971)**	**(0.990)**	**(0.996)**	**(0.999)**
	0.9					**(0.886)**	1.61	10.33	51	707
	0.8					0.43	8.39	45.70	216	2845
	0.7				**(0.669)**	1.58	20.62	102.45	484	5742
	0.6				0.10	3.42	38.52	191.39	896	10548
	0.5				0.36	5.95	62.29	305.44	1456	16442
	0.4				0.72	9.14	91.99	448.06	2113	23998
	0.3				1.13	12.88	127.36	620.93	2932	33312
	0.2				1.48	16.79	166.92	815.20	3845	43695
	0.1				1.42	19.33	203.35	1005.17	19843	54185
0.25	1.0					**(0.947)**	**(0.986)**	**(0.995)**	**(0.998)**	**(1)**
	0.9				**(0.851)**	0.17	2.94	15.19	71	687
	0.8				0.06	1.26	13.22	67.79	287	2906
	0.7			**(0.671)**	0.35	3.33	31.20	152.58	685	7280
	0.6			0.05	0.85	6.42	57.21	279.28	1263	14523
	0.5			0.16	1.54	10.55	91.57	435.38	2049	23001
	0.4		**(0.304)**	0.33	2.42	15.73	134.48	632.62	2971	33760
	0.3		0.0003	0.52	3.44	21.87	185.73	874.06	4050	46448
	0.2		0.01	0.68	4.47	28.61	243.70	1153.56	5391	60899
	0.1		0.000048	0.66	5.02	34.35	299.69	1428.43	6661	75614
1	1.0					**(0.973)**	**(0.993)**	**(0.997)**	**(0.999)**	**(1)**
	0.9			**(0.835)**	**(0.924)**	0.41	4.33	21.39	98	784
	0.8			0.02	0.28	2.09	18.48	82.13	399	4394
	0.7		**(0.691)**	0.13	0.83	5.11	42.92	199.09	950	10530
	0.6		0.03	0.33	1.66	9.53	78.13	358.43	1726	18694
	0.5		0.10	0.62	2.78	15.39	124.56	577.25	2714	30374
	0.4		0.20	0.98	4.19	22.71	182.52	848.91	3938	45016
	0.3		0.31	1.40	5.85	31.43	251.84	1177.78	5528	61446
	0.2		0.41	1.82	7.64	41.20	330.61	1545.13	7193	80855
	0.1		0.39	2.02	9.03	50.25	408.13	1917.83	8906	100766

$k_* K_s^{-1}$	C	t_c (h)								
		$\rho_T = 1$	$\rho_T = 2$	$\rho_T = 3$	$\rho_T = 5$	$\rho_T = 10$	$\rho_T = 25$	$\rho_T = 50$	$\rho_T = 100$	$\rho_T = 300$
5	1.0			**(0.924)**	**(0.964)**	**(0.987)**	**(0.997)**	**(0.999)**	**(1)**	**(1)**
	0.9		**(0.860)**	0.01	0.10	0.73	6.36	32.93	139	911
	0.8		0.02	0.13	0.59	3.27	26.45	128.13	612	6960
	0.7		0.09	0.37	1.47	7.69	60.93	265.90	1269	15815
	0.6	**(0.586)**	0.22	0.75	2.78	14.09	110.47	503.31	2344	27273
	0.5	0.010	0.39	1.26	4.51	22.54	175.71	819.33	3805	41960
	0.4	0.03	0.62	1.89	6.68	33.10	257.15	1187.17	5521	62842
	0.3	0.05	0.87	2.65	9.26	45.71	354.63	1643.30	7611	86045
	0.2	0.07	1.14	3.46	12.13	59.98	465.67	2159.50	9997	112586
	0.1	0.06	1.28	4.09	14.72	73.79	576.13	2679.91	12077	141333
25	1.0		**(0.935)**	**(0.965)**	**(0.983)**	**(0.994)**	**(0.998)**	**(0.999)**	**(1)**	**(1)**
	0.9	**(0.817)**	0.01	0.05	0.21	1.13	9.09	51.78	180	797
	0.8	0.001	0.083	0.266	0.96	4.79	37.32	207.14	739	10800
	0.7	0.02	0.23	0.67	2.28	11.09	85.62	411.12	1790	18965
	0.6	0.05	0.45	1.25	4.19	20.17	154.94	695.03	3291	36337
	0.5	0.10	0.75	2.04	6.72	32.14	246.19	1152.69	5198	60152
	0.4	0.16	1.12	3.02	9.87	47.07	360.08	1675.99	7696	87409
	0.3	0.22	1.56	4.18	13.64	64.94	496.46	2297.32	10608	120290
	0.2	0.29	2.04	5.48	17.90	85.26	652.01	3019.41	13934	157050
	0.1	0.32	2.43	6.65	21.97	105.32	807.50	3897.72	17294	196498

Table 2 – Calculus example of rainfall (ρ_T), soil (t_c) and hillslope geometry ($k_* K_s^{-1}$) parameters (shaded row) considered in the application of the suggested procedure, according to the parameters from which they depend. The critical duration of rainfall, calculated according to two different empirical relationships, $t_{cr}^{(1)}$ and $t_{cr}^{(2)}$, and the corresponding critical rainfall intensity, i_{cr}, when using the classical CIA formula are also reported.

PRESENT SOLUTION						**CIA**	
RAINFALL		**SOIL**		**HILLSLOPE "GEOMETRY"**			
$\langle h_{60} \rangle$ (mm)	**40.94**	**K_s (mm/h)**	**0.72**	**H_{max} (m)**	**324**	**Width (m)**	**200**
st.dev (mm)	**18.96**	**θ_s (cm^3/cm^3)**	**0.55**	**H_{min} (m)**	**241**	Area (m^2)	93282
α (mm^{-1})	0.07	**Ψ_m (mm)**	**199**	S_0	17.8%	Area (ha)	9
u (mm)	32.41	ω (h)	151.3	**L (m)**	**466**	$t_{cr}^{(1)}$ (h)	0.0717
n	**0.36**	**s**	**0**			$t_{cr}^{(2)}$ (h)	0.0718
T (years)	**15.4**			**k ($m^{1/3}/s$)**	**8**	i_{cr} (mm/h)	390.4
P	0.94	**t_p** (h)	0.0057	**n_{Mann} ($s/m^{1/3}$)**	**0.125**		
a_T (mm/h)	72.4			k_*	0.00724		
t_{cr} (h)	0.46						
i_{cr} (mm/h)	118.3						
ρ_T	**100**	**t_c (h)**	**151.3**	**$k_* K_s^{-1}$**	**0.01**		